2017

Development of Laboratory Scale Conical Spouted Bed Reactors

James Blake Gegenheimer
Louisiana State University and Agricultural and Mechanical College

DEVELOPMENT ON LABORATORY SCALE CONICAL SPOUTED BEDS

A Thesis

Submitted to the Graduate Faculty of the
Louisiana State University and
Agricultural and Mechanical College
in partial fulfillment of the
requirements for the degree of
Master of Science

in

The Department of Mechanical Engineering

by
James Blake Gegenheimer
B.S.M.E., Louisiana State University, 2016
May 2017

Dedicated to my mother and father, Mr. and Mrs. David Gegenheimer

ACKNOWLEDGEMENTS

This thesis would not have been possible without the encouragement and support of my major professor, Dr. Ingmar Schoegl. Since beginning of my career in the graduate school, he has been more than generous with making sure I was able to complete my degree in the allotted time. This thesis would not have been possible without his consistent support and input.

I would like to thank the members of my committee, Dr. Ram Devireddy, Dr. Keith Gonthier and Lt Col William Magee. Dr. Devireddy sparked my knowledge in thermal-fluid systems early in my undergraduate career and Dr. Gonthier solidified it through both of their rigorous and challenging lectures.

I would like to thank the Air Force for allowing me an educational delay so that I would be able to complete my master's degree. The Air Force has been generous enough to pay for my undergraduate degree and free me from the financial burdens that allowed me to focus on my academics and attain a master's degree.

I would like to give a special thanks to Charlie Wilson, who gave me constant support and was an amazing resource when writing this thesis. Without him, this work would not be what at the current standard.

I am especially grateful of my parents, David and Kristen Gegenheimer, who have continuously supported me throughout my career and have been willing to give everything so that I may pursue my educational and personal goals. I would not be where I am without the drive that they have always instilled in me.

TABLE OF CONTENTS

LIST OF TABLES

LIST OF FIGURES

ABSTRACT

Conical spouted beds (CSBs) are a form of a fluidized bed that is characteristic of its spouting behaviors. The conical spouted bed has a small inlet that diverges through a conical section towards a larger fixed-diameter column which is filled with static spouting media. By injecting a fluid at a sufficient velocity, a small spout will form in which the spouting media will become entrained by the fluid particles and carried to the top of the system where it will circulate back into the system. It has been shown that CSB reactors have the potential for increasing the heat circulation in fuel reforming techniques used for the production of hydrogen rich syngas. This thesis investigates the design and behavior of a cold-flow laboratory scaled conical spouted bed (CSB) including the effects of system parameters such as the stagnated bed height, inlet diameter, cone angle, particle selection and fluid selection. These parameters were varied through a series of test in which the pressure was measured with respect to the inlet gas velocity to determine the minimum spouting point. Previous correlations are compared to measured data and it was found that these correlations were insufficient at predicting the measured points accurately. This is due to separate parameters being used and scaled differently than the current study. Therefore, a new correlation is presented with an average error of 8.2% - significantly less than that of other correlations. The behaviors found were expected based on the physical hydrodynamic behavior as well as other behaviors being detailed including the effects of internal spouting and unstable spouting. With a fundamental hydrodynamic study complete, the addition of chemical reactions may be introduced to further understand the effects of CSB reactors for more efficient production of eco-friendly fuel sources.

CHAPTER 1
INTRODUCTION

1.1 Research Motivation and Problem Statement

With constant fluctuations in the fossil fuel industry, an increasing demand for alternative energy sources has been a rising concern for the last few decades. Many chemical fuels such as hydrogen and syngas (mixture of hydrogen and carbon monoxide), have processes developed for production, but need further, more efficient developments. A proposal for such a development is for the use of conical spouted bed (CSB) reactors.

The conical spouted bed, as shown in Figure 1 is a vessel that has a small inlet that diverges through a conical section towards a larger fixed-diameter column which is filled with static spouting media. By injecting a fluid with enough momentum, a small hollowed channel, that has similar dimensions to the inlet diameter, can form. Once the fluid exists the channel formed by spouting media, it will diffuse rapidly into the larger column region. As spouting media fall from the annular region into the core, they are carried by the fluid to the top of the bed where they will fall back into the column or annular region creating a circulatory pattern.

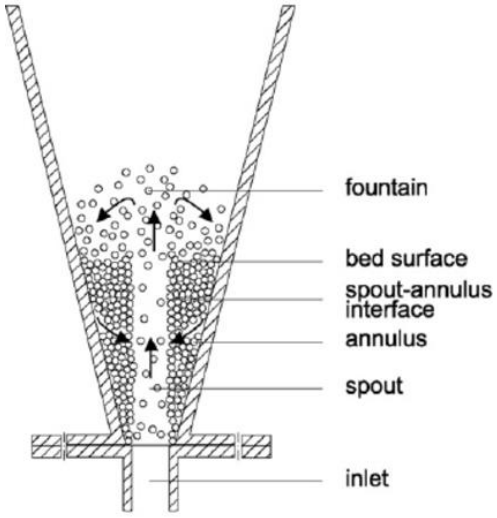

Figure 1: CSB Fountain Geometry [1]

A CSB may be used for fuel production by utilizing fuel reforming techniques in its core. The introduction of a spouting media can further promote heat transfer in the particles from the dense fluid-particle interaction giving it an advantage over traditional reactors. However, before this study can begin, an investigation into the hydrodynamic behavior of CSBs must be performed without the occurrence of chemical reactions. To simulate the high temperature flow that would occur in a CSB reactor, different gases will be used to vary the fluid density and viscosity – the predominant fluid properties affecting the hydrodynamic CSB behavior.

The particular point of interest is the minimum velocity required for spouting as this point yields the largest gas residence time (time in which the fluid and spouting media are in contact) while providing solid particle circulation. While a multitude of correlations for the minimum spouting velocity can be found in current literature, none of the experimental apparatuses used were scaled comparably to the current research needs [2, 3, 4, 5, 6, 7, 8, 9]. It is therefore the goal of this study to develop a non-diminsionalized correlation that accurately predicts velocity required to achieve stable spouting. A range of solid particle sizes and densities, gases, inlet diameters, and bed heights will be used to frame the correlation. With the development of an analytical correlation and sufficient trends, this work may be used to further research into the development of small scale CSB reactors used for fuel reforming techniques such as pyrolysis.

1.2 History

Fluidized beds have been in use in industry since 1879 with applications such as ore roasting, drying of grains and pneumatic conveying in which particles can be circulated into a system where the fluid momentum pushes particles through to a collection port at the top. In the process of particle transport, the particles may be dried or heated by the fluid based on its physical properties [10]. The idea of the spouted bed, a subset to the fluidized bed, was first

introduced to the research community by Gishler and Mathur in 1954 at the National Research Council of Canada (NRCC) as a denser solid phase alternative [11, 12]. The fluidized bed was insufficient for drying of wheat particles as the wheat was less characterized in shape and had a mean particle size too large for fluidization, where of slugging, an unwanted phase of fluidized beds, would often occur [12]. It was at this point that the NRCC initiated further research and found that the spouted bed "appears to achieve the same purpose for coarse particles as fluidization does for fine materials" [13]. However, as the application of spouted beds have widened in the 50 years since, this has been shown to not be the case as fluidization and spouting having separate features that will be discussed in the next section [14].

Spouted beds gained much more popularity in 1959 with the book titled Fluidization in which the spouted bed was introduced as its own chapter [15]. Since then, over 1300 works have been published with a variety of applications, such as: coal combustion, solid blending, cooling, granulation and coating, electrolysis in liquid spouted beds and drying of grains and evaporative solutions [14, 16, 17]. In more recent years, there has been a major shift from using spouted beds for industrial purposes towards laboratory experiments where the effectiveness of various purposes can be accurately studied.

1.3 Fluidized and Spouted Bed Characteristics

The fluidized bed and spouted bed have similar features and have been used to achieve similar results until only recently (1954-present) with findings showing each variation exceling at separate task [14]. The fluidized bed is a very general term that characterizes a multitude of sub-systems where it utilizes multi-phase mixing in which a gas is sent through a solid spouting media similarly to the spouted bed. The most classic fluidized beds use finer spouting media (20-

600μm), larger gas inlet offices and smaller particle densities (1.4-4g/cm^3) in which the goal is not to not create a spout, but to entrain the particles in a fluidized state [18].

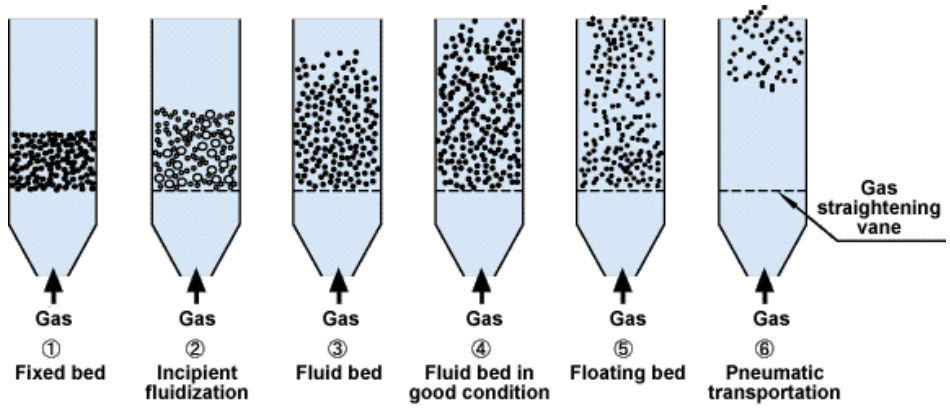

Figure 2: Typical Flow Phases Found for a Fluidized Bed [19]

Depending on the momentum of the fluid, the bed can have multiple phases of solid-fluid interaction as shown in Figure 2. These phases generally include: incipient fluidization, a fluid bed, a floating bed and pneumatic transportation. As discusses previously, when larger, coarser, and less characterized particles were placed into fluidized beds the fluid momentum was not sufficient in creating a fluidized state giving birth to the conventional spouted bed.

The conventional spouted bed is based on a cylindrical cone that diffuses to a fixed diameter column as shown in Figure 3. Conventional spouted beds require higher flow rates due to spouting media being located at a pre-determined height in the column. The conical spouted bed (CSB), a variation of the conventional bed is a newer field of study that has been developed as the research needs of spouted beds has evolved [21]. CSBs, as seen Figure 1, have spouting media located only in the conical region of the bed allowing for larger, courser and less uniform spouting media to be used compared to the conventional spouted bed [13].

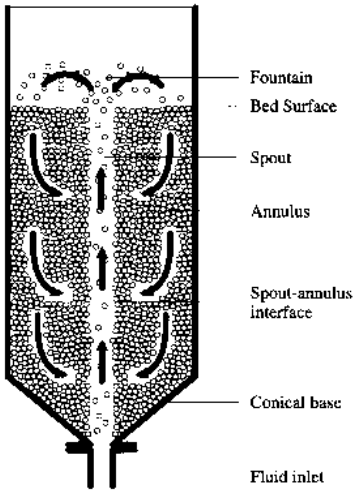

Figure 3: Typical Spout Produced in a Conventional Spouted Bed [20]

Though these coarser, larger particles create a more chaotic and random motion, it also increases the circulation of the particles which can allow for shorter gas-solid contact, or residence time, useful in certain applications [21]. Due to these modifications of the CSB, it has been shown to be more useful in applications such as coal gasification, pyrolysis, and catalytic polymerization [22, 23, 24, 25, 26]. Additional features of CSBs include less particle segregation compared to a fluidized bed. However, while particle segregation is a positive feature that could reduce the residence time of the gas, it can also be a challenge when agglomeration occurs due to fusing particles [27, 28, 29, 30].

1.4 Thesis Structure

Now that the basic structure of the conical spouted bed has been detailed, more specific topics may be addressed. Chapter 2 will be a literature review describing the fundamentals of spouting. It will describe the system and flow regimes commonly found as well as the hysteresis observed. The hysteresis is the separate paths taken by the fluid between the ascending and descending velocity processes and the separate spouting point that can be achieved as a result.

While it is important to understand both aspects, the descending process will be used as the scope of the research as it is the absolute minimum velocity required for spouting as discussed in Chapter 2. Unstable spouting will also be discussed as it should be taken into account when designing the test parameters for the CSB. The chapter will end with existing empirical correlations that can be found in the literature.

Chapter 3 will deal with the methods used to build and test the CSB. Included is the design used for the control system to create an automated process to operate testing. Experimental parameters will also be explained in greater detail and how they vary compared to the existing literature. Data processing is discussed in the determination of the minimum spouting velocity and the statistical methods used to determine the validity of the results.

Chapter 4 will describe the results found from testing. This includes comparing results to existing correlations and the accuracy and precision of the results. An empirical correlation based on measured results is also presented where each parameter is discussed on its effect to the minimum spouting velocity. Other topics in this chapter include instabilities found in certain testing parameters and internal spouting. Chapter 5 will end with conclusions of the work and future recommendations when the next phase of research begins utilizing fuel reforming techniques.

CHAPTER 2
SPOUTING FUNDAMENTALS

With the introduction of the CSB in 1954, an assortment of literature has been published that detail the behavior and physics of the CSB from a variety of contexts. This chapter is essentially a literature review and will focus on the previous trends and results found and their importance to accomplishing the goals of the current research. These topics include the system description and flow regimes followed by other possible CSB features including unstable spouting, internal spouting and the pressure drops felt across the bed. All of these aspects must be studied to understand the geometric specifications to which the CSB should be built as well as proper parameter selection. These aspects will also be important to understand the physical meaning behind the results that will be presented in Chapter 4.

2.1 Flow Regimes

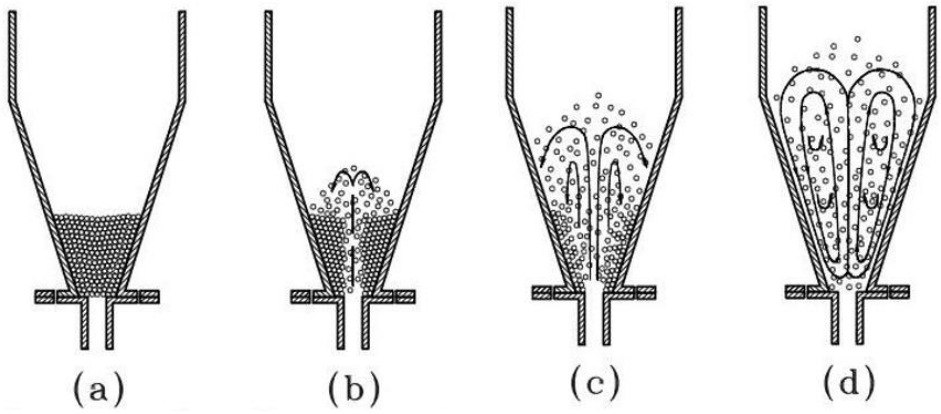

Figure 4: Spouting regimes for different inlet velocity: fixed bed (a), stable spouting operation (b), transition regime (c), and jet spouting (d) [2]

As the gas inlet velocity is increased, an evolution will occur in the spouting media as shown in Figure 4. This evolution is described as happening in four dominant flow phases. The first phase, a static or fixed bed, would be found at low flow rates where the fluid momentum is insufficient to break through the spouting media. At a sufficient fluid momentum, a channel will form breaking through from the base of the CSB to the top of the bed of particles thus creating a stable spout. The spout will create a circulatory pattern in the spouting media where the particles agglomerate on the walls where they diffuse to the hollowed core and are then carried to the top of the channel by the fluid momentum [14].

The third, or transition, phase is not as well characterized compared to the first two phases. This phase is the intermediate process between the formation of the spout and the fourth phase, jet or dilute spouting. The last phase is characterized when there is no agglomeration of particles on the conical walls of the CSB. While jet spouting is similar to a fluidized state, significant differences still exist between a CSB and fluidized bed. A fluidized bed is characterized by the solid particles acting in a state of disorder while the jet spouting phase still has a circulatory pattern as seen in (d) of Figure 4. It should also be noted that additional bubbling and slugging phases can exist at higher bed heights in the conventional spouted bed. These phases are undesirable for most applications as they are non-uniform and non-axisymmetric giving the conical spouted bed an advantage over the conventional spouted bed [14].

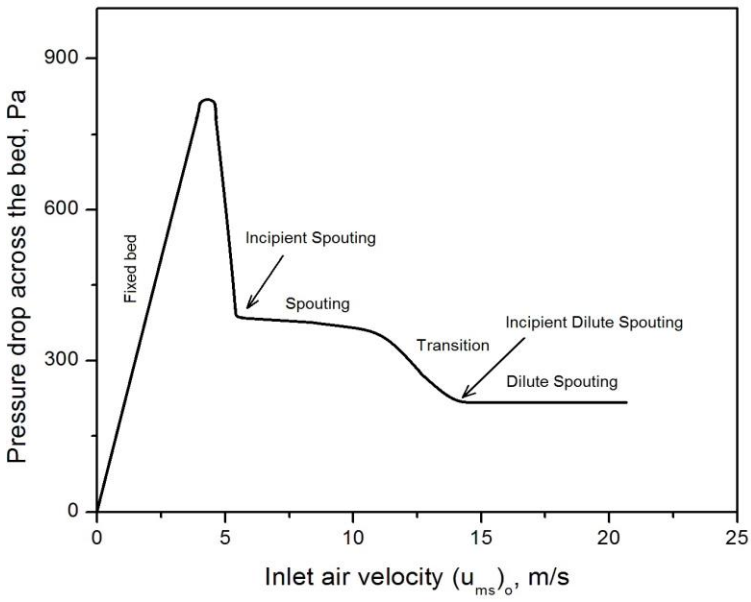

Figure 5: Theoretical Pressure-Velocity Curve for CSB [31]

While Figure 4 shows a visual representation of the spouting phases, the most common method used to determine the phase is not by visual means, but by measuring the pressure with respect to fluid velocity which yields Figure 5. The spouting phase is characterized at the end of the peak pressure drop, or at approximately 5m/s in this example. The transition region is much less defined as it happens over a range of inlet velocities eventually leading to jet or dilute spouting. It is often found that the transition region is even less noticeable than seen in Figure 5 making it difficult to decipher [4, 32, 33]. Visual determination can even be more reliable in some cases depending on instrument sensitivity. Also notice the pressure drop across at the formation of spouting or pressure needed to break through the bed of particles represented as the breaking

Further, other aspects of Figure 5 also do not portray a perfect representation of the phase diagram. The individual geometry of each apparatus can cause deviations in the pressure curves; however, it is accepted as a theoretical curve one would expect to obtain.

2.2 Flow Hysteresis

Similar to the concept of a static and dynamic coefficient of friction, flow hysteresis is present in CSBs creating a separate ascending and descending process with respect to the gas velocity. The hysteresis is caused due to channeling in the bed, or the internal spout evolution. As the fluid momentum forges a path through the spouting media, a compacted dome at the top of the bed is formed as a product forcing particles to an unpacked state from the bottom up and therefore, causing more resistance. On the other hand, the uncompacted dome (particles collapsing from an unpacked circulatory state to a packed state) transpires when the channeling bed is decreasing where the particles become packed from the top down which causes less resistance [34, 35]. Put simply, it is easier to let the particles be packed together from the top down, than unpacked from the top up.

The resulting change in resistance can be evident through a reduced frictional pressure drop and a reduced minimum velocity. Further studies from Wang, interrupted the spout in the ascending process and dropped it to a lower value to find that the pressure drop was discontinuous and began to follow the descending path [34]. Near similar effects were found when interrupting the descending process, but the original ascending pressure was never reached. Whether ascending or descending, once the process was placed back on the correct path, it returned to the original pressure thus confirming the internal spouts role in the flow hysteresis. Both ascending and descending paths will converge once the spout has been formed due to flow hysteresis being a function of the internal spout alone [14, 34].

2.2.1 Internal Spouting

As previously stated, an internal spout must develop before external spouting can occur. However, the degree of internal spouting is dependent on the explicit geometry of the CSB. Stagnated internal spouting, or internal spouts that remain in place for a moderate range of flow rates, can have a role in the formation of the external spout and the observed pressure drop [34]. Most literature points to pressure curves seen in Figure 5, in which the peak pressure is the onset of internal spouting and the lack of a further drop in pressure represents the fully realized external spout [7, 33, 5, 36, 37, 38]. In these cases, internal spouting is rapid, but some authors have found internal spouting to happen over a wider range [2, 3, 4, 32].

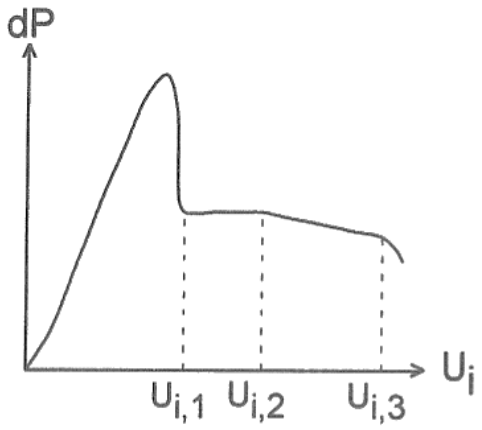

Figure 6: Pressure Curves Found for Gorshtein (1964) [34, 2]

Gorshtein and Mukhlenov found the onset of external spouting ($U_{i,2}$) to be located after the frictional pressure drop (Figure 6), once transitional spouting occurred [2]. In this case, an external spout has formed with the peak pressure drop and remained stagnated between $U_{i,1}$ and $U_{i,2}$ until the external spout formed. Note that the pressure drop representing external spouting significantly smaller and can almost be overlooked compared to the internal spout.

2.2.2 Peak Pressure Drop

While multiple pressure drops occur over the flow regimes of CSBs, the maximum pressure drop occurring between the onset of internal and external spouting is a point of interest as it is an indicator of the internal friction and spouting. Unlike the onset velocity of external spouting, the related pressure drop is a contested facet in the spouted bed field. Mukhlenov and others have made obvious positive correlations between bed height and the peak pressure drop; however, this has been contested by Olazar and Gelprin who have received criticism for their negative correlation [3, 38, 39, 14]. Other contested points include cone angle and the role it plays [40, 41]. There also seems to be objections into the repeatability of the peak pressure drop. While Wang found that the descending peak pressure drop was repeatable, this was not the case for the ascending process giving way to the idea that the initial packed state of the bed is crucial to the frictional pressure drop occurred in the ascending process [34]. Some studies have gone into further depth in the formation of internal spouts by measuring the pressure gradient at various heights from the inlet diameter to the maximum bed height [40].

It should be noted that the order of magnitude of peak pressure drop expected for the current experiment scale is ~1kPa. This change in pressure would correspond to a 1% change in fluid density and temperature for air and comparably small amounts for other fluids. Coupled with large pressure drops found upstream to drive the flow, the peak pressure drop is not in the scope of the current study in a quantitative manner; rather, the essential trends will be analyzed.

2.3 Geometric System Description

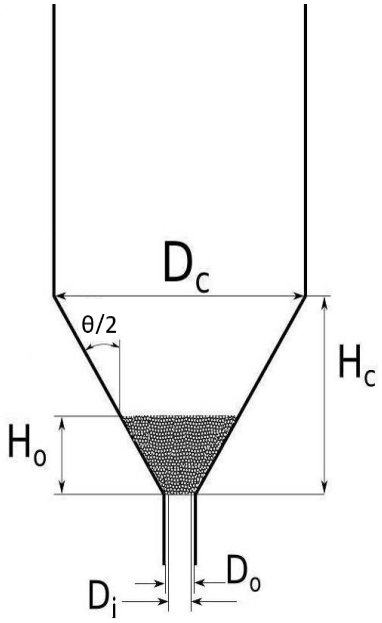

Figure 7: CSB Geometry [31]

A range of parameters exist that characterize the CSB and can be groups into three categories: geometric, fluid, and spouting media properties. Figure 7 shows the standard nomenclature used to represent the geometric parameters. D_i represents the diameter of the inlet air pipe while D_0 represents the inlet diameter of the cone which may be separate values. H_0 represents the stagnated bed height of the particles. If $H_0 > H_c$, then the system is described as a conventional spouted bed, whereas for this study, $H_0 < H_c$ so the system remains defined as a conical spouted bed (CSB). D_c is the diameter of the column.

The fluid properties used include the viscosity (μ) and density (ρ) while the spouting media is characterized by the particle density (ρ_p) and mean particle diameter (d_p). Combined, these properties characterize the CSB with a well followed nomenclature in the literature.

2.4 Unstable Spouting

The phenomenon of unstable spouting is also a condition to be considered in spouted beds and commonly happens for two reasons. The first is due to the periphery of the external spout continuously opening and closing while the second is due to spouting media sinusoidaly collapsing into the core of the spout [14]. Though these features are separate and unique, a combination of the two is most common as they are near indistinguishable without the assistance of an optical study.

Unstable spouting is undesirable as it interrupts the normal circulation of the spouted bed and is more difficult to determine from the pressure due to high fluctuations from the continuously opening and closing spout. Certain factors have been shown to affect the spouting velocity in which the main focus is the geometric conditions of the CSB [7]. These factors include the ratio of D_i/d_p, D_i/D_o, θ, and a maximum spoutable bed height and will be discussed below.

2.4.1 Inlet Diameter/Particle Diameter Ratio (D_i/d_p)

Mathur found strong differences between conventional and conical spouted beds in the inlet diameter/particle diameter ratio (D_i/d_p) [35]. For conventional beds, this ratio was said to be less than 30 for stable spouting while 2-60 for conical beds. This hints that this nondimensionalized factor may be a weak function of stability in CSBs as compared to conventional beds. This also supports the idea that CSBs can use a larger variety of particle sizes.

2.4.2 Inlet Diameter/Cone Bottom Diameter (D_i/D_o)

It was found by Olazar that a minimum and maximum value exist for the inlet diameter/cone diameter (D_i/D_o) [7]. A minimum intuitively exists due to flow separation – a dead space for the fluid created from the sudden expansion. Seemingly, this can create circulatory

issues at the base of the spout causing instabilities [42]. The minimum ratio was found to be 0.5 while a maximum was found to be 0.83. However, an upper limit is not as intuitive as the lower limit. Olazar stated that this limit may be exceeded, but will be less likely in producing a stable spout [7]. This effect is due to non-agglomerating particles at the base of the discontinuity of the inlet diameter.

2.4.3 Cone Angle

Intuition can once again lead to a minimum cone angle to produce spouting. A cone angle of 0° would results in a straight column which would hinder the circulation of any particles and defeat the purpose of the spouted bed by creating a fluidized bed. Instability, however, is a factor in the CSB due to larger, coarser particles. The lower limit has been found to be 28° by Olazar and was confirmed by Sharma at 30° in the previous study at LSU with a model scaled exactly as the current study [7, 31]. It should be noted that while an upper limit does not exist, higher angles (approaching 180°) provide little to no circulation also defeating the purpose of the spouted bed [14].

2.4.4 Maximum Spoutable Bed Height

While the phases of slugging and bubbling beds were avoided in CSBs compared to conventional beds, it can still occur if the bed heights are sufficiently large and have larger particle sizes. While a quantitative correlation has not been deduced, qualitative correlations state that the maximum spoutable bed height increases as: particle diameter decreases, D_i/D_o decreases, and the cone angle increases [43]. Due to the small scale nature of the apparatus used in the current study, the maximum spoutable bed height was never of serious concern.

2.5 Existing Correlations for Minimum Spouting Velocity

A multitude of correlations can be found to determine the minimum spouting velocity for conical spouted beds. A non-diminsionalized Reynolds number ($(Re_{ms})_0$), is generally used with a power law curve fit with non-diminsionalized parameters. Table 1 shows the correlations that will be used as a reference in this study. A parameter occasionally used, but not specified to this point is D_b, or the diameter of the spouting media at the bed height of H_0. This can easily be determined from geometry of the system.

Table 1: Existing Spouting Velocity Correlations [2, 3, 4, 5, 6, 7, 8, 9]

Source	Correlation
Bi et al. (1997)	$(Re_o)_{ms} = [0.30 - 0.27/(D_b/D_o)^2]\sqrt{Ar\,(D_b/D_o)[(D_b/D_o)^2 + (D_b/D_o) + 1]/3}$
Choi (1992)	$(u_o)_{ms} = \sqrt{2gH_o}\,0.147\left((\rho_p - \rho)/\rho\right)^{0.477}(d_p/D_c)^{0.61}(H_o/D_c)^{0.508}\,(D_o/D_c)^{0.243}$
Gorshtein (1964)	$(Re_o)_{ms} = 0.174\,Ar^{0.5}[1 + 2\,\tan(\gamma/2)\,(H_o/D_o)]^{0.25}\,\tan(\gamma/2)^{-1.25}$
Markowski (1983)	$(Re_o)_{ms} = 0.028\,Ar^{0.57}\,(H_o/D_o)^{0.48}\,(D_c/D_o)^{1.27}$
Mukhlenov (1965)	$(Re_o)_{ms} = 3.32\,Ar^{0.33}(H_o/D_o)^{1.25}\,\tan(\gamma/2)^{0.55}$
Sharma (2011)	$(Re_o)_{ms} = 717.26\,(Ar)^{0.08}\,(H_o/D_o)^{0.85}\,(d_p/D_o)^{1.23}$
Tsvik et al. (1967)	$(Re_o)_{ms} = 0.4\,Ar^{0.52}(H_o/D_o)^{1.24}\,\tan(\gamma/2)^{0.42}$
Olazar et al. (1992)	$(Re_o)_{ms} = 0.126\,Ar^{0.5}(D_b/D_o)^{1.68}\,\tan(\gamma/2)^{-0.57}$ $d_p > 1$ mm
Olazar et al. (1996)	$(Re_o)_{ms} = 0.126\,Ar^{0.39}(D_b/D_o)^{1.68}\,\tan(\gamma/2)^{-0.57}$, $d_p \leq 1$ mm

The characteristic length used for the Reynolds number is d_p leading too:

$$(Re_{ms})_0 = \frac{(u_{ms})_0 d_p \rho}{\mu} \tag{1}$$

The Archimedes number is a parameter classically used to characterize systems of different fluid densities and has been modified to be used in gas-solid mixed systems with the following correlation:

$$Ar = \frac{g{d_p}^3 \rho(\rho_p - \rho)}{\mu^2} \tag{2}$$

Based on Table 1, there is significant deviation from correlation to correlation [2, 3, 4, 5, 6, 7, 8, 9]. This can be most accurately explained by the wide variety of system geometries and spouting media used in each respective experiments as shown in Table 2.

Table 2: Parameters of Various Correlations Found in Table 1

Source	Particle size (mm)	D_0 (mm)	D_c (mm)	D_i (mm)	θ (deg)	H_o (mm)	H_0/D_0
Markowski	3.41 - 10.35	5.6 - 300	300 - 1100	5.6 - 300	37	3.36 - 690	0.6 - 2.3
Choi	2.1 - 2.8	21 - 35	240 - 450	38	60	240 - 400	6.86 - 19.05
Olazar	0.95 - 25	30 - 60	360	60	28 - 45	70 - 300	0.33 - 6.67
Bi et al.	1.16	12.7 - 25.4	65 - 95.8	38.1	30 - 60	80 - 335	3.15 - 26.38

CHAPTER 3
METHODS

Before testing could begin, the CSB had to be designed based on the guiding principles to avoid instability discussed in Chapter 2 which include the ratios of D_i/D_o, D_i/d_p, and θ. Testing parameters were then chosen and expanded based on the previous study by Mandeep Sharma in 2011 where only D_0, H_0 and d_p were varied [31]. The test parameters were expanded to vary ρ_p, ρ, μ, and θ as well as create an automated system to control the test and continuously operate the system for multiple cycles. The control system consisted of a mass flow controller and pressure transducer to study the system.

Once the automated system was complete, measurements were taken in which the procedure will be discussed along with the definition and methods used to determine the minimum spouting velocity. Once measurements were completed, they were compared to other correlations found in the literature (Table 1) in which the statistical methods will be discussed.

3.1 CSB Design

In terms of the physical apparatus used for the CSB, only two parameters would be changed regularly – D_i and θ. Therefore, the CSB was subdivided into two portions consisting of a base and conical section. While these two pieces could be built in one continuous design, separating them allows for more efficient manufacturing as D_i and θ could be matched independently.

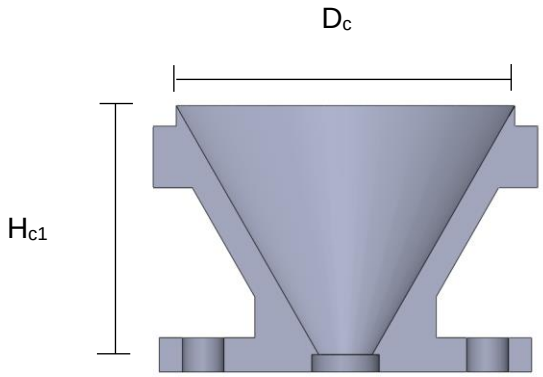

Figure 8: Conical Section of the Designed CSB

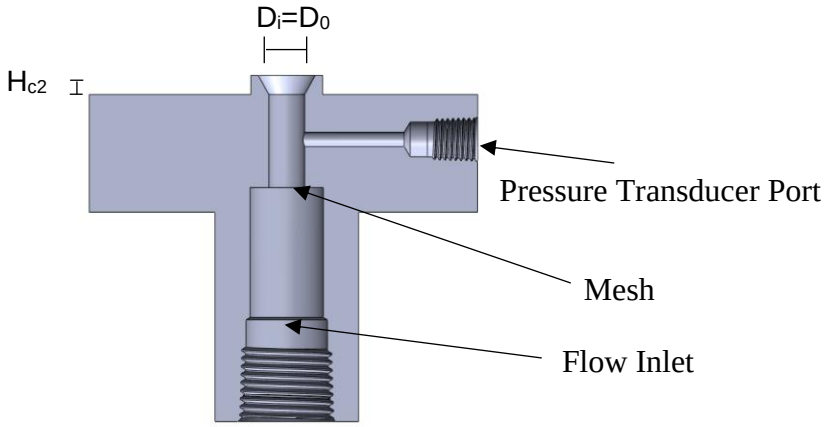

Figure 9: Base Section of the Designed CSB

The conical piece is the cone of the CSB while the bottom houses the pressure transducer port, flow inlet and establishes the inlet diameter as seen in Figure 8 and 9. Two conical sections were made for two separate cone angels (45° and 60°) and 4 bottom pieces for 3.30mm, 4.47mm, 6.0mm, and 6.35mm. The diameter of the cylindrical section, D_c, was determined to be 69.85mm, or 2 3/4". The total height of the cone, or maximum height particles can be placed in the system is the addition of H_{c1} and H_{c2}. Because D_c was held constant, the maximum height of the particles is dependent D_i and θ. The CSB was designed such that a maximum height of 50mm

can be reached for and D_i and θ. Further, a mesh will be placed at the location shown in Figure 9 so that the spouting media does not travel into the flow inlet pipe.

3.1.1 CSB Production

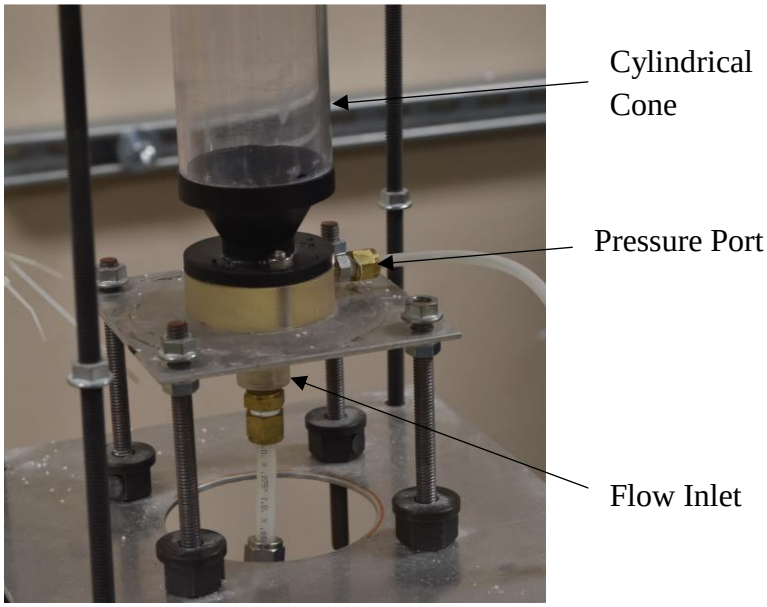

Figure 10: Final CSB Design and Testing Apparatus

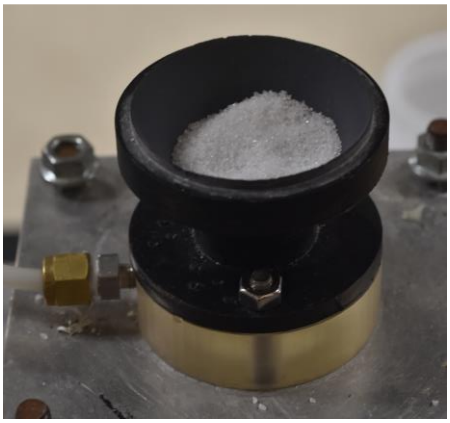

Figure 11: Final CSB Design with Spouting Media

Since the scope of the study is cold flow, 3D printing was used for ease of manufacturing. Classic fused deposition modeling, or plastic extrusion was not an option in the printing due to leaks being present when running simple gases through the system. Stereolithography was used

instead with a FormLabs printer in which no leaks would be present. The accuracy of the prints range from 0.1-0.5mm depending on the axis of printing [44]. These accuracies are significant when made on the inlet diameter; therefore, the inlet diameter was measured with the measured value being used if differing from the design. Figure 10 shows the testing apparatus used for the CSB while Figure 11 shows the inside of the conical section with spouting media inserted.

3.2 Control System

While multiple control systems exist that could perform the required task, an Arduino Uno was chosen based on simplicity [45]. A program was designed to govern a mass flow controller while reading the pressure transducer while writing the data onto an SD card. While this section gives a brief overview of the data acquisition system, a more detailed analysis can be found in Appendix A.

3.2.1 Mass Flow Controller

A mass flow controller (Omega, Inc.) was used in which the volumetric flow rate ranged between 0-100L/min. The reported error is 0.25L/min, though for low flow conditions (<3L/min) the error seen was much larger [46]. Due to this factor, a separate flow controller would need to be used if the minimum spouting flow-rate entered this range.

Based on the Arduino pulse width modulation (PWM) that was used to govern the mass flow controller, it could be increased in 20mV increments giving the controller a resolution of 0.4% of the total flow rate. Preliminary testing found that this was insufficient as too few data points were taken across the pressure drop observed at the spout formation. Therefore, a digital to analog converter (DAC) was used in which the resolution was increased to 1mV increments, increasing the resolution from to 0.02% increments of the total flow rate [47].

3.2.2 Pressure Transducer

A Barometric pressure sensor (SparkFun Electronics) was used due to a high accuracy for a low cost. The sensor has a reported accuracy of 10Pa while the experimentally observed error was closer to 25Pa [47]. The sensor was hermetically sealed in a PVC structure with a line running to the pressure port located on the base of the CSB.

3.3 Experimental Parameters

The previous study conducted by Mandeep Sharma took a total of 30 data points across a narrow range of parameters. A goal of this study was to increase the parameters of the cone angle, fluid density and viscosity and the particle density. Table 3 shows the parameters that have been expanded to the current study and will be discussed in the following sections.

Table 3: Parameter Comparison Between the Previous and Present Study [31]

Source	Particle size (mm)	Particle Density (kg/m^3)	D_0 (mm)	D_c (mm)	θ (deg)	H_o (mm)	Gas
Previous Study	0.483, 1.092	3920	3.302, 4.572, 6.35	69.9	60	10 - 50	Air
Present Study	0.483, 0.686, 1.0, 1.092	2002 - 3520	3.30, 4.47, 6.0, 6.35	69.9	45, 60	10 - 70	Air, Argon, Helium

3.3.1 Spouting Media

Two types of particles were used for the spouting media to vary the density. The first was an aluminum oxide lapping grain with a reported density of 3950 kg/m^3 [48]. Though the density of solid aluminum oxide is 3950 kg/m^3, the material was found to be internally porous in which the working fluid did not percolate through the surface. Therefore three separate density values could be found for the three particle sizes were chosen consisting of 483μm, 686μm, and 1092μm. These values are reported in Table 4. The second particle chosen was a porcelain

finishing media with a density of 2418 kg/m^3 and a particle size of 1mm [48]. From these parameters, the Archimedes number ranges from 15,919-183,969.

Table 4: Spouting Media Properties

Particle Composition	Particle Diameter (mm)	Density (kg/m^3)
Aluminum Oxide	0.483	3520
Aluminum Oxide	0.686	3380
Aluminum Oxide	1.092	3340
Porcelain	1	2418

3.3.2 Stagnated Bed Height

The stagnated height of the spouting media was varied in 10mm increments between 10mm and 50mm for most experiments in the 60° cone due to 50mm being equal to H_c. If a higher height was used, the system would become a conventional spouted bed, which is not in the scope of this study. The 45° was able to achieve higher heights at 70mm before the column was reached due to the steeper angle.

3.3.3 Working Fluid

Three gases were used in the study: Air, Argon, and Helium, as to vary the gas density and viscosity as shown in Table 5. By changing these fluid properties, the Archimedes number was varied to study low density flow. This flow can simulate a flow under elevated temperature which is the subsequent goal of the study.

3.3.4 Inlet Diameter

The inlet diameter was varied between 4 separate values: 3.30mm, 4.47mm, 6.0mm, and 6.35mm. While the original scope of the study was to study only three diameters, a misprint at 6.0mm occurred allowing additional data to be taken. Table 5 shows a summary of all parameters changed in the CSB.

Table 5: Changing Parameters for Current Study

Parameters	Symbol	Range	Units
Diameter of particle	d_p	0.483, 0.686, 1.0, 1.092	mm
Diameter of inlet air pipe	D_o	3.3, 4.47, 6.0, 6.35	mm
Diameter of the upper part of the cone	D_c	69.85	mm
Diameter of the lower part of the cone	D_i	3.302, 4.47, 6.0, 6.35	mm
Diameter of column	D_c	69.85	mm
Height of the cone	H_c	55.04 – 80.4	mm
Cone angle	θ	45, 60	deg
Stagnated height of bed	H_o	10 – 50, 10 – 60, 10 – 70	mm
Minimum spouting velocity at D_o	$(u_{ms})_o$	4.9 – 139.9	m/s
Reynolds number at minimum spouting	$(Re_{ms})_o$	156.7 – 1296.8	-
Archimedes number	Ar	14615 – 183969	-
Density of particles	ρ_p	2002 – 3520	kg/m^3
Fluid Density	ρ	0.1664, 1.184, 1.661	kg/m^3
Fluid Viscosity	μ	1.96, 1.81, 2.23 x 10^{-5}	Pa s

3.4 Data Acquisition

Once all parameters were set, the automated process was started in which the controller would ramp the data from zero flow, to the prescribed value. Once the peak flow was reached, it would ramp the flow back down to zero flow conditions and begin the process again. This was repeated five times minimally to establish error. Due to flow hysteresis, it is important to differentiate between the ascending and descending results. For this study, the descending results will be used as it is the absolute minimum point at which spouting can be achieved as discussed in Section 2.2. A more comprehensive description of the process used to acquire data is detailed in Appendix A.

3.5 Data Processing

3.5.1 Spouting Velocity Determination

Once the data were recorded, the corrected pressure and set velocity were used to determine the minimum spouting velocity. Calibrations for the pressure transducer found a systematic drift that would occur. Though the drift was unquantifiable with exact precision, corrections that assumed linearity between the beginning and ending of each test were found to dampen the effect and therefore, a corrected pressure was calculated. The pressure measurements were corrected at the beginning and end of each cycle where zero flow conditions occurred and the gauge pressure was known to be zero. At larger velocities, the static pressure would eventually decrease below atmospheric conditions due to an increased dynamic pressure. For this reason, the stagnation pressure was used instead so that only the pressure losses felt across the bed would be observed.

$$\Delta P_0 = (P - P_i) - \left[\frac{P_i - P_e}{2\,V_{max}}\right] V + \frac{\rho V^2}{2} \tag{3}$$

The calculation used to determine the pressure loss across the bed is presented in Equation 3 where ΔP_0 represents the stagnation pressure, P and V represent the concurrently measured pressure and velocity, V_{max} represents the maximum velocity the system was tested towards, and P_i and P_e represent the pressures at the beginning and ending of the test.

It should be noted that independent of the pressure value used (gauge, corrected, or stagnation), the pressure drop observed from the spout formation will be clearly visible (as it happens over a narrow range of velocities (~1m/s)) and will not change in location. Therefore, the minimum spouting point is independent of the pressure formulation used.

While there are multiple values that can be used for the pressure, the velocity is the simpler, independent variable. Two velocities were recorded including the set and measured velocity. The set velocity is the commanded value given to the flow controller while the measured velocity is the value the controller reads back to the system. These values should be one and the same, but the measured value can have small fluctuations from noise. The set value and was used over the measured velocity to reduce this noise. Similarly to the pressure, minimum spouting point is independent of the velocity value used. For all data, the set and measured velocities were calibrated to verify that there were no deviations.

Once the velocity and corrected pressure were recorded for each test, they were sent through a digital low pass filter in MATLAB where the noise was reduced to produce a continuous curve [49]. The filter is described in detail in Appendix A. At this point the minimum velocity was able to be determined.

Throughout the literature, there are a multitude of methods to determine the spouting velocity as discussed in Section 2.2.2 [2, 3, 4, 33, 36, 5, 7]. Nevertheless, the results will be near similar. For this study, the definition of the minimum spouting velocity is at the center point of the external spouting pressure drop. This point is defined as average between the maximum and minimum second derivatives of pressure or where the curvature has peaked. Due to miniscule discontinuities still being present after the filtering process, these points were determined visually.

$$(U_{ms})_0 = \frac{U\left(\frac{d^2P}{du^2}\right)_{min} + U\left(\frac{d^2P}{du^2}\right)_{max}}{2} \quad (4)$$

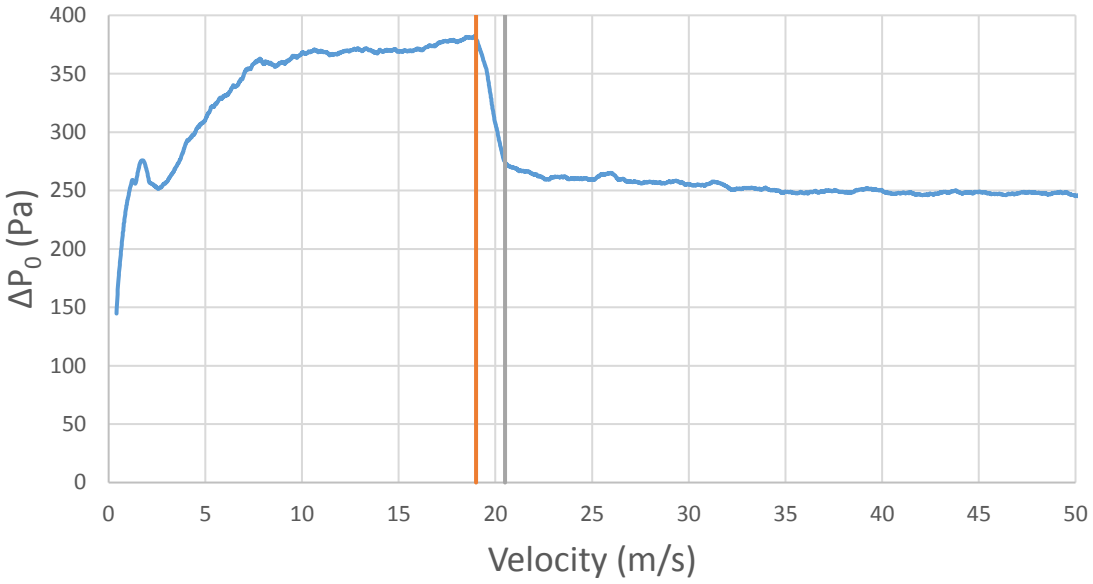

Figure 12: Typical Pressure Curve found in the study (H_0=50mm, D_0=6.35mm, θ=60°, d_p=686 µm, Gas=Air, ρ_p=3950)

Figure 12 shows an example of one such graph in which the minimum spouting velocity was determined to be 19.9m/s.

3.6 Sources of Uncertainty

Error is a serious concern in any study and how it is reported. For this study, measurement error is reported based on a 95% confidence interval which leads to the question: what has caused the error? The first aspect is instrumentation, a source of error always found. The two other major aspects of error are in the minimum velocity determination and the spouting media. Each source of error is important to understand not only by the uncertainty, but if the uncertainty is stochastic which is random with a mean of 0, or systematic, having a nonzero mean.

3.6.1 Instrumentation Uncertainty

The first aspect of error is to discuss instrumentation uncertainty. The reported uncertainty of the flow controller is ±0.25L/min with a resolution of 0.01L/min which would translate to ±0.132m/s (D_0=6.35mm), ±0.266m/s (D_0=4.47mm) and ±0.488m/s (D_0=3.30mm) uncertainty across the separate D_0 values used.

The pressure transducer also added to the error by a reported ±12 Pa with a resolution of 1 Pa giving the overall uncertainty as ±12.04 Pa This uncertainty was felt intensely at low bed heights where the maximum pressure drops were <50 Pa, inevitably causing data at low bed heights to be discarded as a spouting point was not discernable. At higher bed heights, a systematic drift in the pressure transducer led to more uncertainties mainly being the path of the pressure loss across the bed after the spouting point was reached. However, the minimum spouting point is nearly independent of these uncertainties as the shape of the pressure curve is more important than the absolute value of the pressure itself.

3.6.2 Spouting Point Determination Uncertainty

Error is also present from the spouting point determination. This point was determined based on visual representation leading to some amount of human error. The author determined every spout across the data for consistency. Additional error is present from the separation across the pressure drop. The separation (usually 1 – 2m/s) is caused by the internal spout beginning to chisel a path through the spouting media towards the bed height. Additional uncertainty is added due to the human aspect of determining the maximum and minimum peaks twice per observation.

3.6.3 Spouting Media Uncertainty

An additional error noted is that found from the spouting media in which the aluminum oxide and porcelain have separate error sources. The aluminum oxide grains lost mass due to attrition throughout the five test that were performed. This is evident from a fine powder accumulating in the cylindrical column over time. A clear trend also exist across all aluminum oxide test showing that the minimum spouting velocity will decrease between tests 1 – 5. The rate at which the velocity decreased was found to be scaled to the bed height, or amount of particles in the system, inferring that all particles were losing mass. This was discovered early in testing and particles were therefore discarded after being run to avoid a change in particle size and further error.

Figure 13: Static Cling Observed by Porcelain Particles

The porcelain particles did not have an issue of mass loss, but instead, static cling. Interactions between the air, porcelain and plastic surface of the CSB led to a small amount of static cling in which only the smaller particles were affected. Based on observation, the static cling seemed to occur throughout all 5 test and therefore, no positive or negative trend is evident in the minimum spouting velocity. This will effectively reduce the bed height by a factor of z

($H_0 - z$) and may possibly interrupt the circulatory motion. This could make significant effects at lower bed heights; however, test for porcelain were only done at high bed heights ($H_0 > 40$mm) due to less resolution based on instrument error. Therefore the static cling is not expected to be a significant source of error found in the observable data.

3.7 Statistical Methods

In the results, the correlations that are currently present in literature will be compared to the measured values obtained from experiments. Therefore, standard statistical tools must be used to properly analyze and discuss the results. There will be two methods used which are confidence intervals and the Student's t variables, which are related, but used in separate manners.

$$\text{Error} = \pm t_{v,P} \frac{s_x}{\sqrt{N}} \tag{5}$$

Most tests taken, were repeated 5 times to establish a sample standard deviation. Since the sample size is finite, the standard error, or sample standard deviation by the square root of N, is multiplied by the Student's t variable which provides an additional coverage factor. This term represents a precision interval, or probability in which the data will fall. For the error calculated for data points, a t variable representing 95% probability was used.

$$\text{Confidence Interval} = \pm t_{v,P} \frac{s_{yx}}{\sqrt{N}} \tag{6}$$

The confidence interval is shown above in Equation 6 and is very similar to the error used in Equation 5. The difference is the confidence interval will be used in regression analysis over a series of data points to determine the wellness of the fit.

$$t = \frac{\sum(y_i - x_i)}{\sqrt{N} * S_{(y_i - x_i)}} \tag{7}$$

In another circumstance, a two-tailed paired t-test will be used which is represented in Equation 7. The paired t-test tests the probability of the difference between two correlations [50]. In this case, it will be used to measure the applicability of previous correlations found compared to measured data. y_i is represented as the predicted value from other correlations while x_i is the measured value obtained in the study. $S_{(yi\text{-}xi)}$ is the standard deviation of the difference. The difference is expected to be 0 if the correlation perfectly represents the given data. Based on the t-value, the probability of the difference (p=p (t, N)) can be found. Low p-values indicate a strong probability that there is difference between the groups of data. For example, p=0.001 would indicate 0.1% probability of correlation between the data sets, or a 99.9% probability that the values, are not the same.

CHAPTER 4
RESULTS AND DISCUSSION

The results were obtained based on the methods presented in Chapter 3 including testing procedure and analytical methods. The raw data results (84 total data points) will first be presented and discussed. The results will then be compared to existing correlations to determine the accuracy in using these correlations to predict the measured values. A power law fit is then presented and discussed on each parameters contribution to the minimum spouting velocity.

Other trends are also presented and discussed on the effect of the minimum spouting velocity. These effects include internal and unstable spouting as well as system error.

4.1 Minimum Spouting Velocity

To first introduce the minimum spouting velocity, we will examine a few examples of the pressure curves obtained and what the results indicate. Raw data will then be presented as a function of bed height with the appropriate error and trends to indicate expected correlations to be found.

4.1.1 Pressure Curves

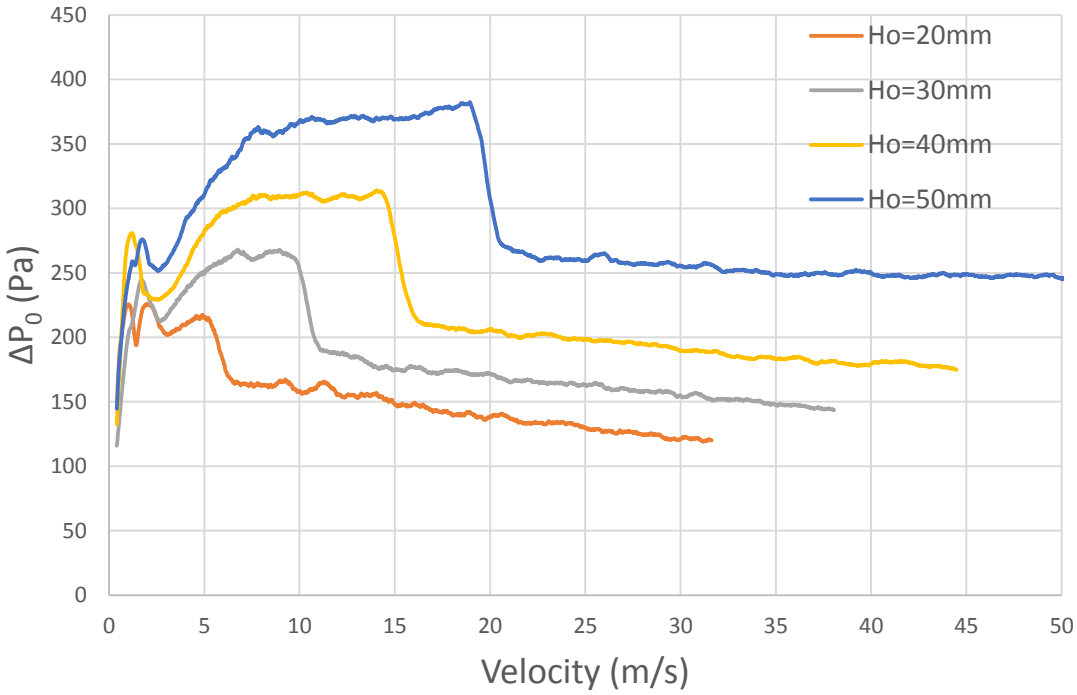

Figure 14: Pressure Curve for D_0=6.35mm, θ=60°, d_p=686µm, Gas=Air, ρ_p=3950kg/m^3

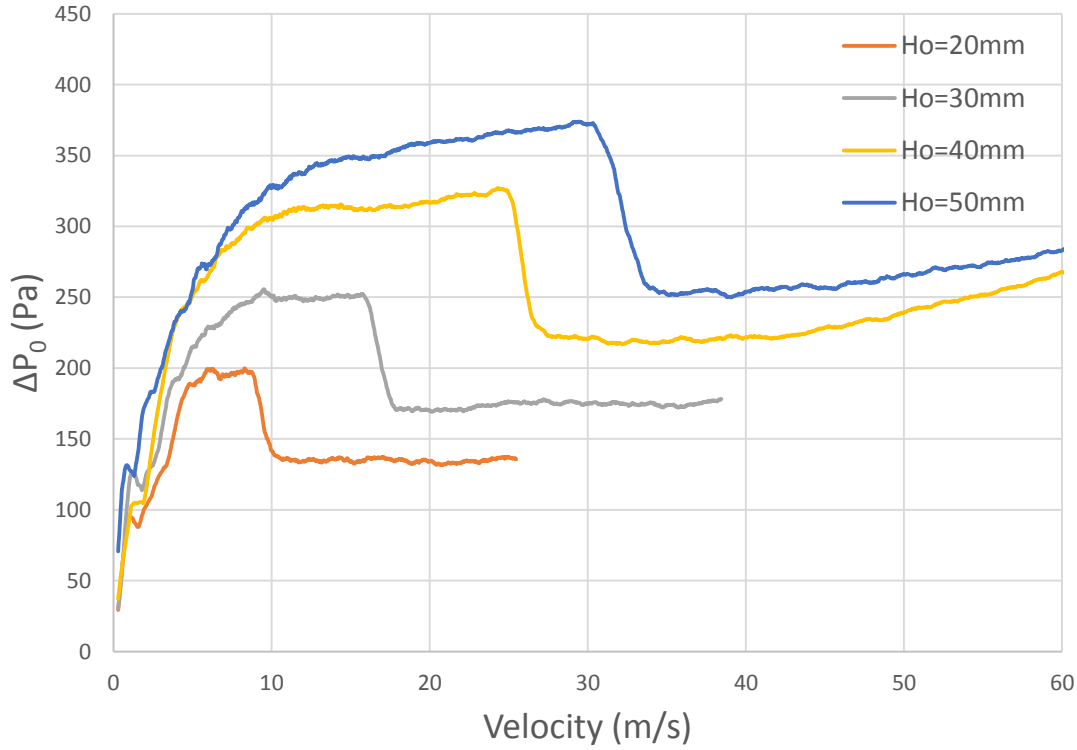

Figure 15: Pressure Curve for D_0=4.468mm, θ=60°, d_p=686µm, Gas=Air, ρ_p=3950kg/m^3

As shown in Figure 12, pressure curves are used to determine the minimum spouting velocity from the stable pressure drop. Examples of these curves are shown in Figure 14 and 15 where all parameters excluding the stagnated bed height were held constant. The major pressure drop is apparent and increases in location as the bed height increases, as expected. The path the curves take is expected to be horizontal or a decrease. The paths taken by the 40mm and 50mm bed heights in Figure 15 show that the stagnation pressure increases with an increasing velocity. This is attributed to the pressure drift experienced in the pressure transducer which will not alter the minimum spouting point.

In the lower velocity ranges, separate peaks can be seen which represent internal spouts being formed. These pressure drops formed from the internal spouts were actually much higher than shown, but were short-lived causing them to be filtered out by the low-pass filter. Nevertheless, these peaks all occur at near similar points which could infer that internal spouting is a weak function of the bed height.

4.1.2 Minimum Velocity as a Function of Bed Height

The following section will contain the raw data found and the error associated with that value. The data are presented as a function of bed height and organized by other changing variables. Trend lines are also included as a power law to show the effect bed height has on the minimum spouting velocity. The trend lines are averaged across each plot to be the average trend. This is done so that in cases of low statistical significance, i.e. where only two data points were taken, there is more certainty in the found results.

4.1.2.1 Aluminum Oxide Spouting Media, Air, 60° Cone Angle

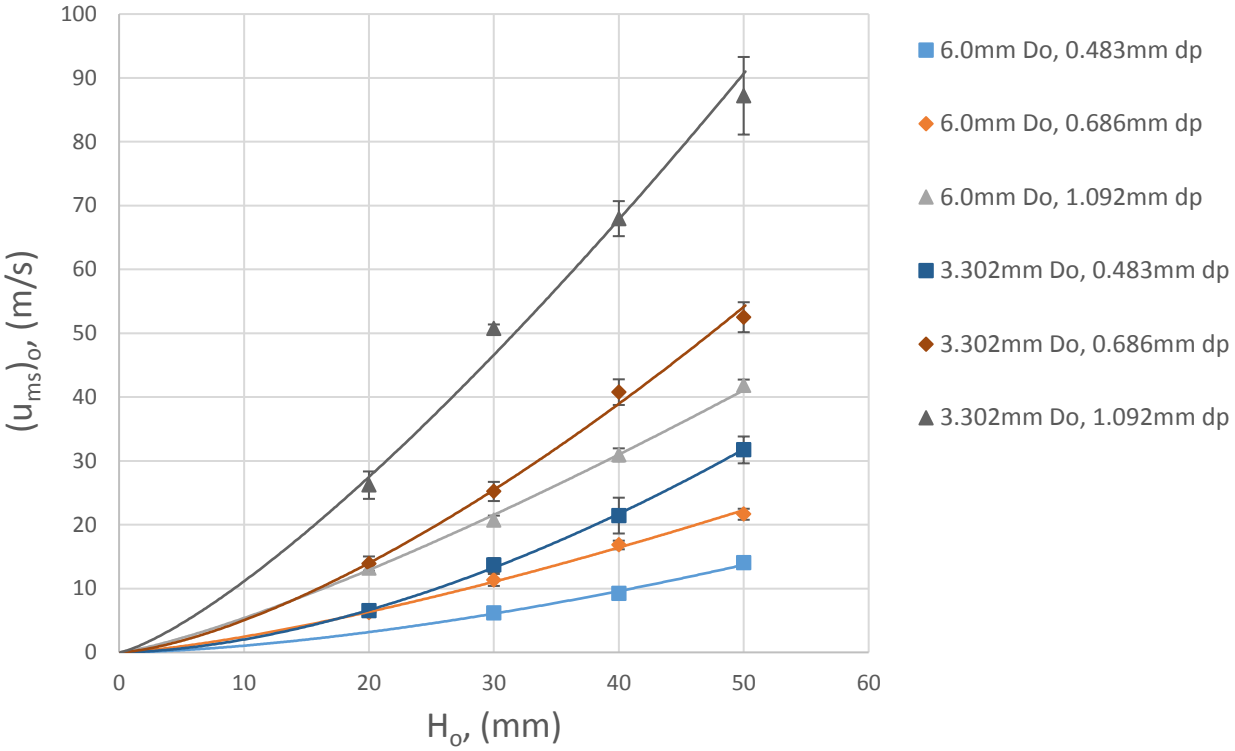

Figure 16: Results for θ=60°, Gas=Air, Aluminum Oxide Particles

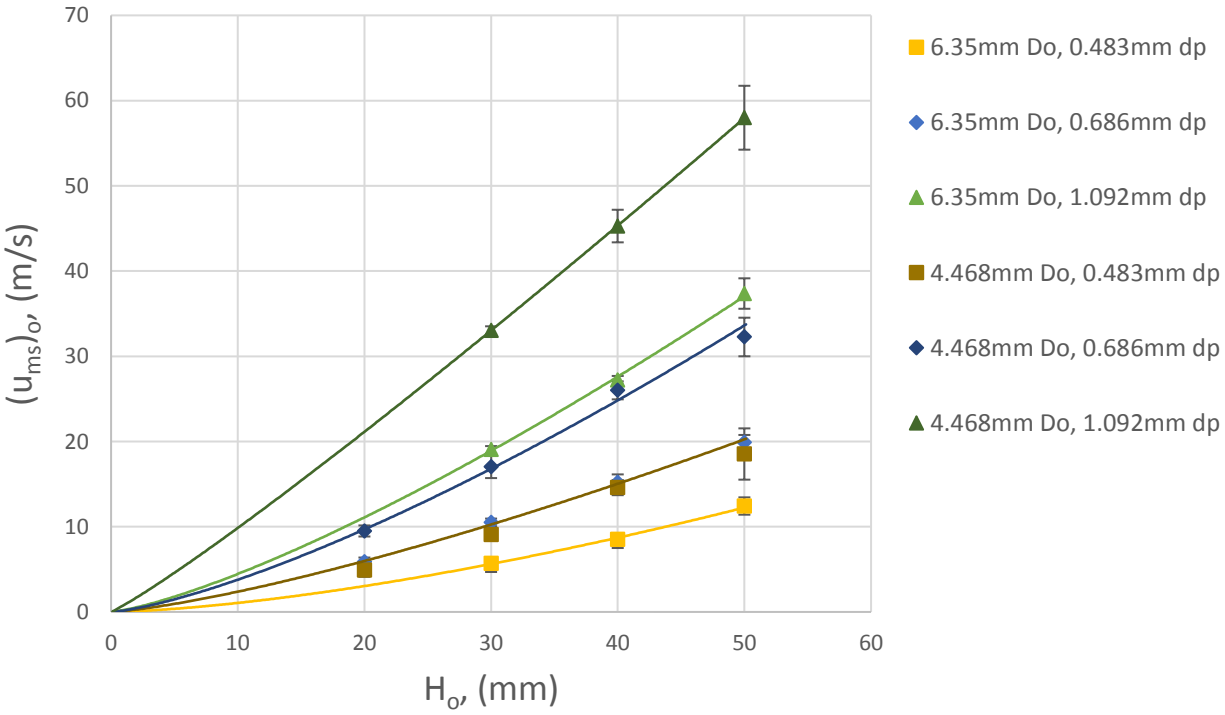

Figure 17: Results for θ=60°, Gas=Air, Aluminum Oxide Particles

The most extensive data was taken for a cone angle of 60° with air as the working fluid and aluminum oxide particles as the spouting media as shown in Figure 16 and 17. Due to uncertainty in the pressure transducer a discernable pressure drop was not always observed at the lower bed heights. For this reason, data was not used at H_0=10mm where the pressure drops were low. Some data for H_0=20mm also had this issue and were not included.

4.1.2.2 Porcelain Spouting Media

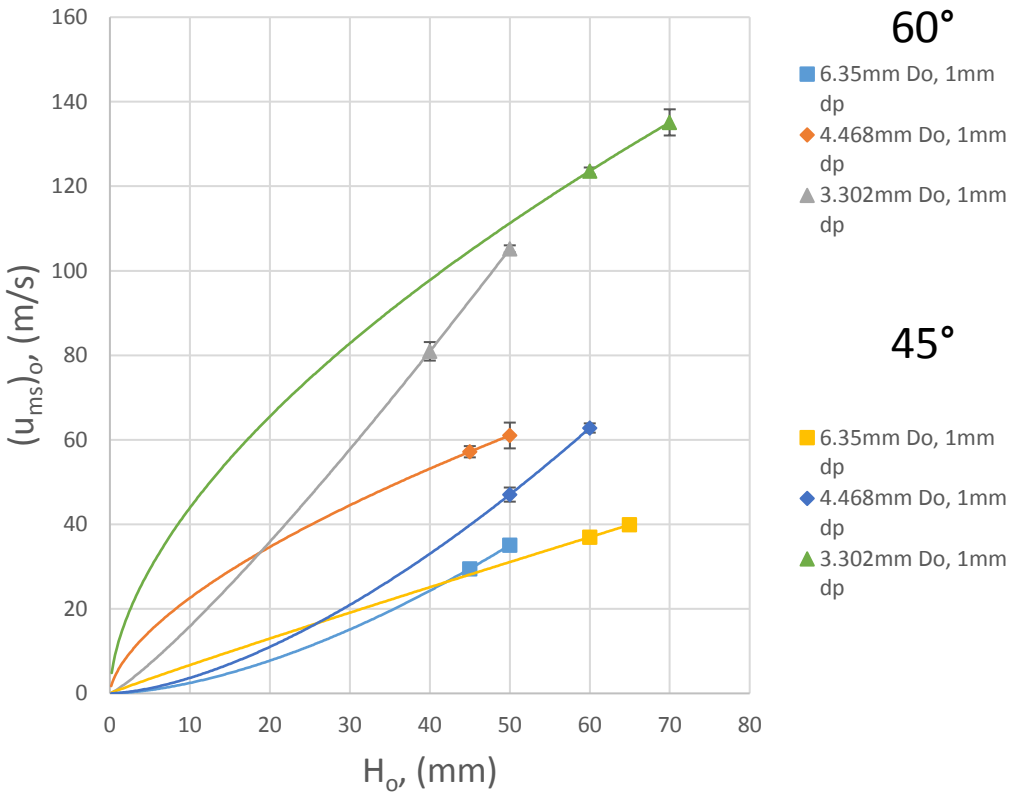

Figure 18: Results for Gas=Air, Porcelain Particles

Figure 18 shows data taken for the porcelain spouting media. Though a range of particle sizes can be found with the only mean particle diameter being 1mm, all particles are spherical compared to the less characterized shape of the aluminum oxide. This may cause the state of packing to be different than that of the aluminum oxide grains which can change the internal

friction as the air may have a separate resistance when traveling through the bed. The porcelain media was found to have smaller frictional pressure drops when compared to the aluminum oxide. Only higher bed heights could be tested when the pressure drop reached was observable.

It is also observed that the power law has exponential values greater and less than one. While this has been reported in previous data, it does not fit with other testing results [5, 31]. Since there are few data points that are also near each other, there is much less certainty in the result compared to other Figures. The reason data points were only taken at higher bed heights is due to the resolution of the external spout being difficult to discern for porcelain particles.

4.1.2.3 45° Cone Angle

As shown in Figure 19, the 45° cone angle had data taken at bed heights up to 70mm. This is due to holding D_c constant, therefore allowing for higher heights. Two data points were taken at a minimum so that a fit could be determined.

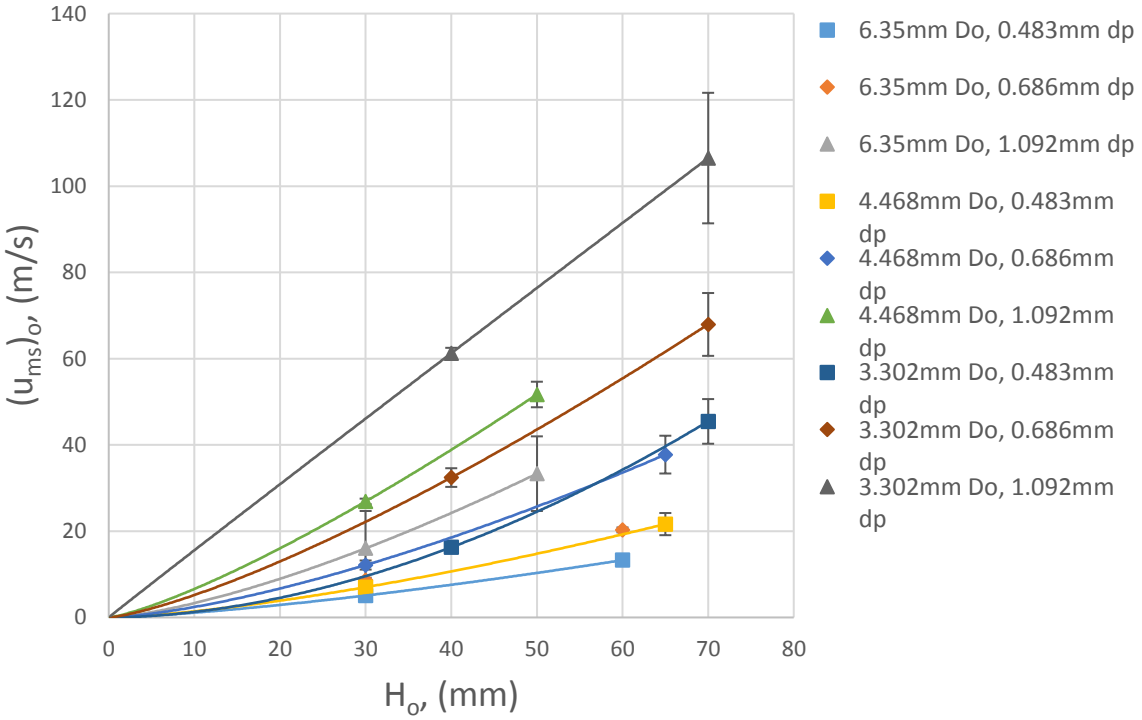

Figure 19: Results for θ=45°, Gas=Air, ρ_p=3950kg/m^3

4.1.2.4 Helium and Argon

Helium and argon were chosen as separate fluids to use in addition to air for the cost and fluid properties. Helium was used to simulate flow at elevated temperatures due to its lower density and viscosity. Testing results from argon found that it behaved near similar to air as the minimum spouting velocities were practically identical which can be attributed to similar physical properties.

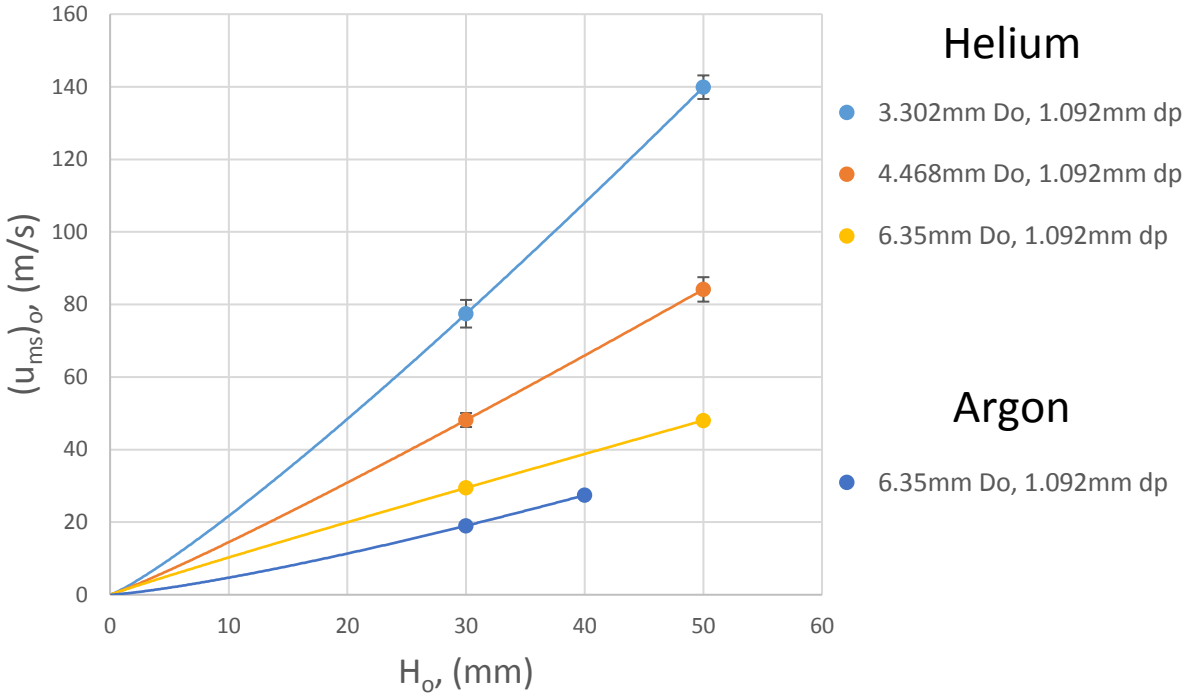

Figure 20: Results for θ=60°, Aluminum Oxide Particles

4.3 Evaluation of Correlations for Minimum Spouting Velocity

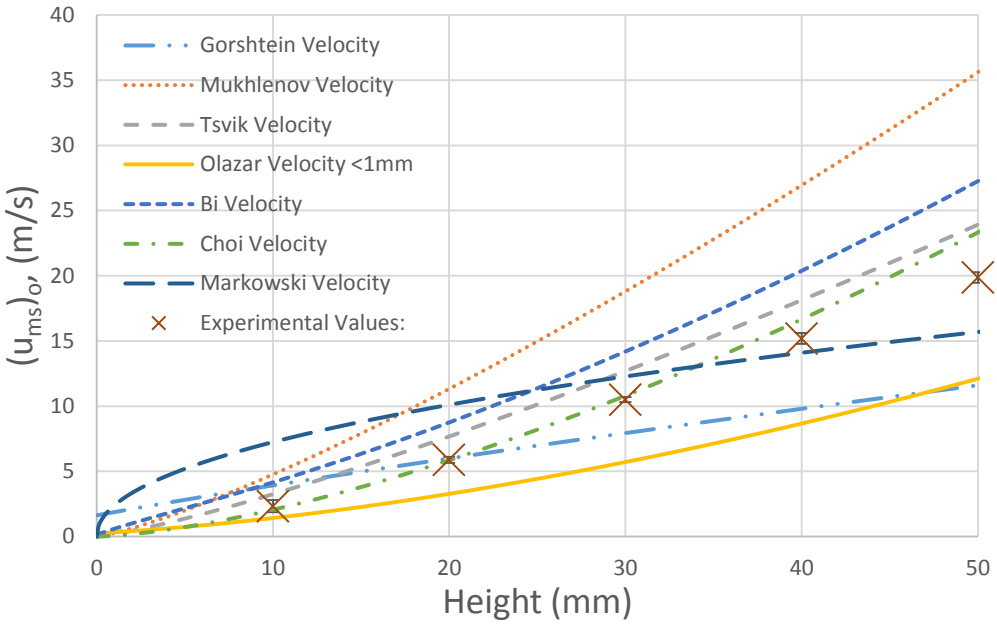

Figure 21: Various Correlations Predictive Power Compared to Measured Results

It was originally hypothesized that the correlations listed in Table 1 would be insufficient in estimating the minimum spouting velocities required for the current CSB due to the inconsistencies found across the fits – leading to the motivation behind this research. However, the question still remains as to the applicability of the fits. Figure 21 gives insight by examining a 60° angle, 6.35mm inlet diameter, air as the working fluid, and a 686μm spouting media particle size for varying stagnated bed heights and the evolution different curves take with respect to the data. While Choi's prediction method may be accurate in Figure 21, this is only a small representation of the large data set and is insufficient when examining the big picture.

As shown in Figure 22 – 29, a visual representation is given into the error found in other correlations. Unity is plotted as the straight horizontal line and represents the accuracy of the data. A curve fit was also applied to get an idea of data precision along with 50% confidence intervals.

Table 6: Figures 23-30 Legend

6.35mm=D_0, Air, θ=60°, Aluminum Oxide	
6.0mm=D_0, Air, θ=60°, Aluminum Oxide	
4.47mm=D_0, Air, θ=60°, Aluminum Oxide	
3.30mm=D_0, Air, θ=60°, Aluminum Oxide	
Argon, θ=60°, Aluminum Oxide	
Helium, θ=60°, Aluminum Oxide	
Air, θ=60°, Porcelain	
6.35mm=D_0, Air, θ=45°, Aluminum Oxide	
4.47mm=D_0, Air, θ=45°, Aluminum Oxide	
3.30mm=D_0, Air, θ=45°, Aluminum Oxide	
Air, θ=45°, Porcelain	

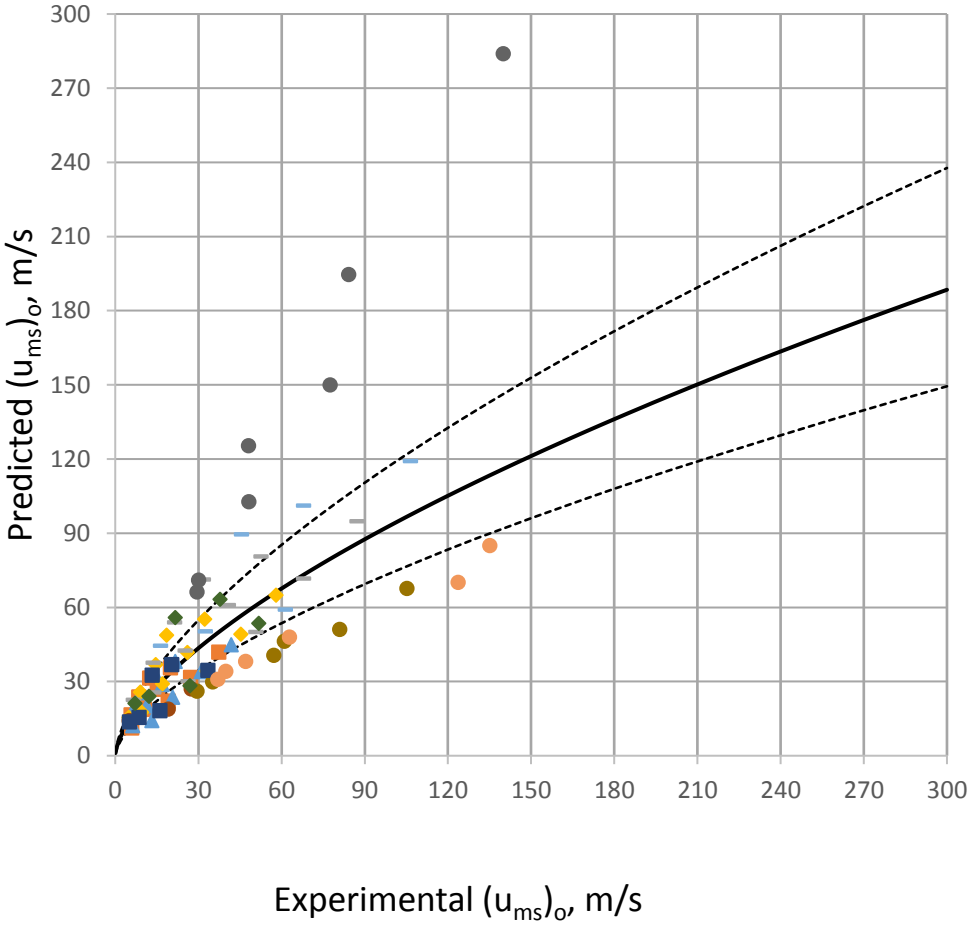

Figure 22: Mukhlenov Correlation

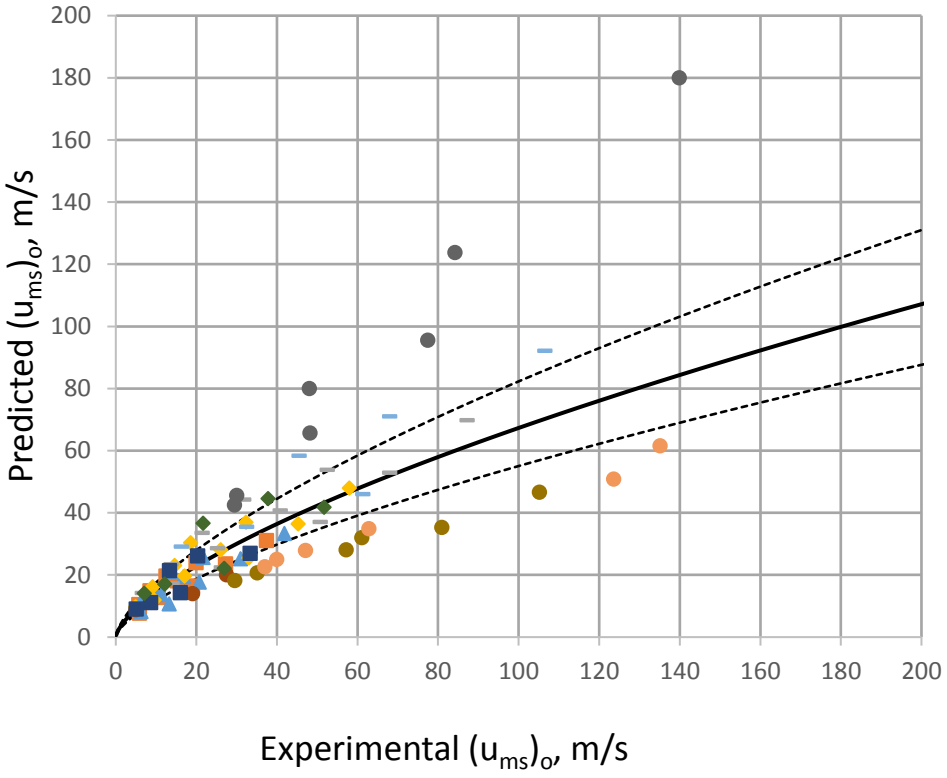

Figure 23: Tsvik Correlation

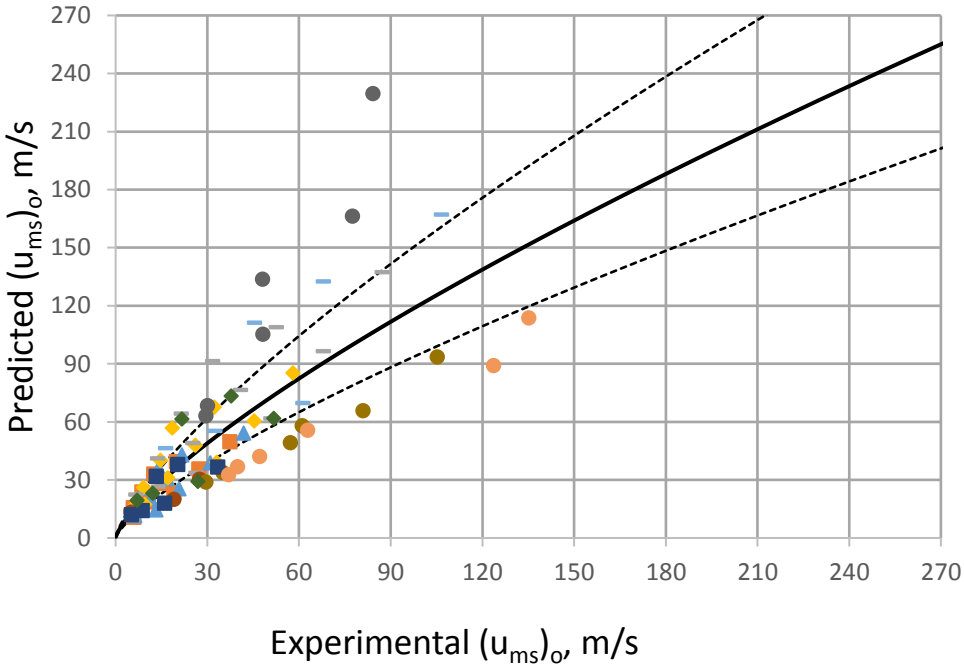

Figure 24: Olazar Correlation I

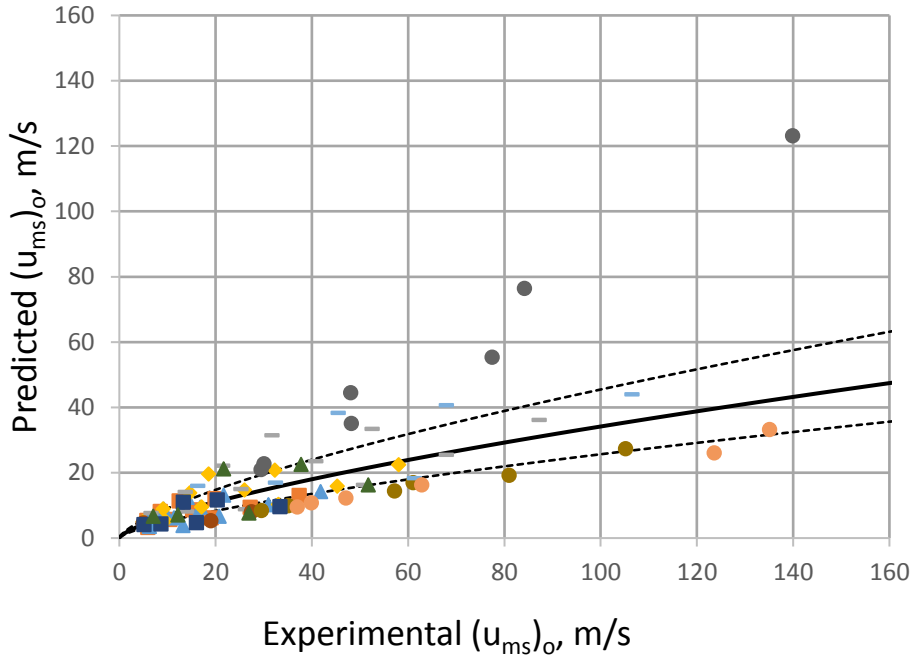

Figure 25: Olazar Correlation II

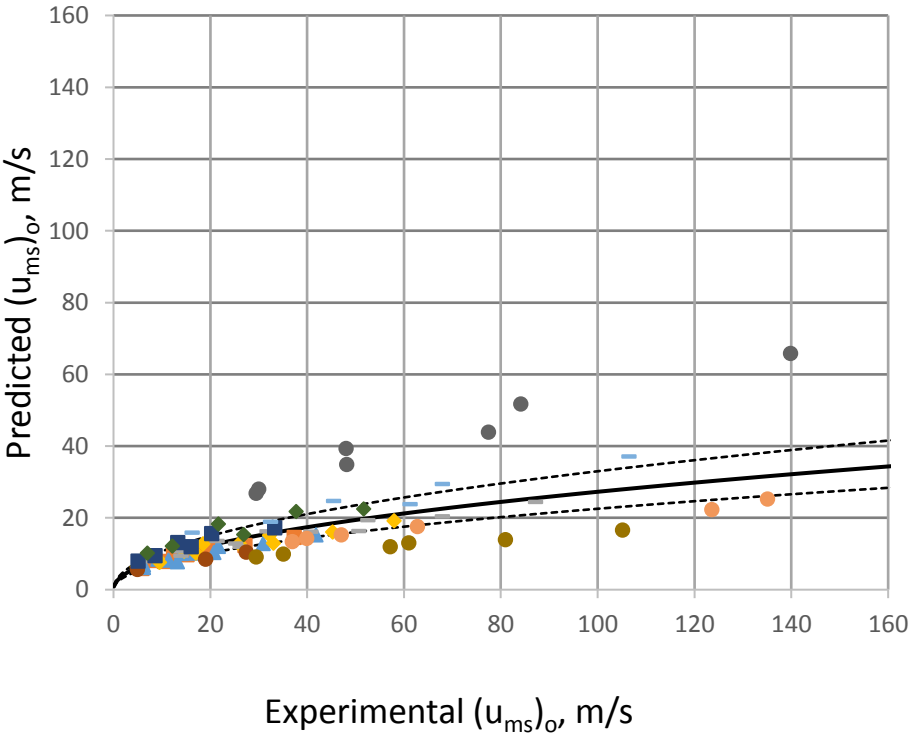

Figure 26: Gorshtein Correlation

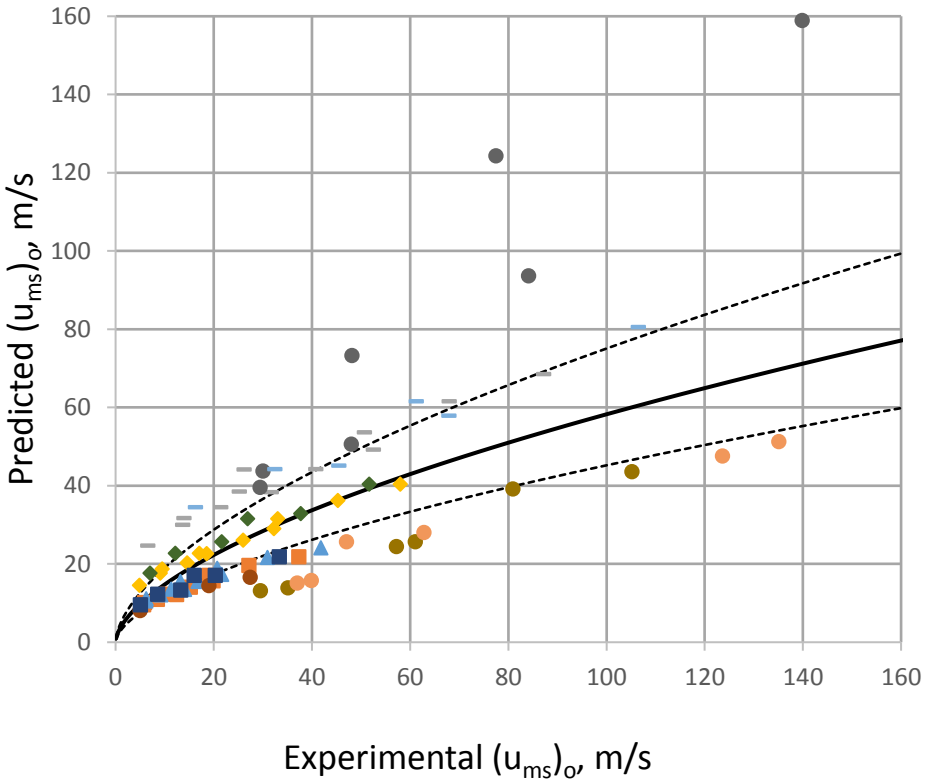

Figure 27: Markowski Correlation

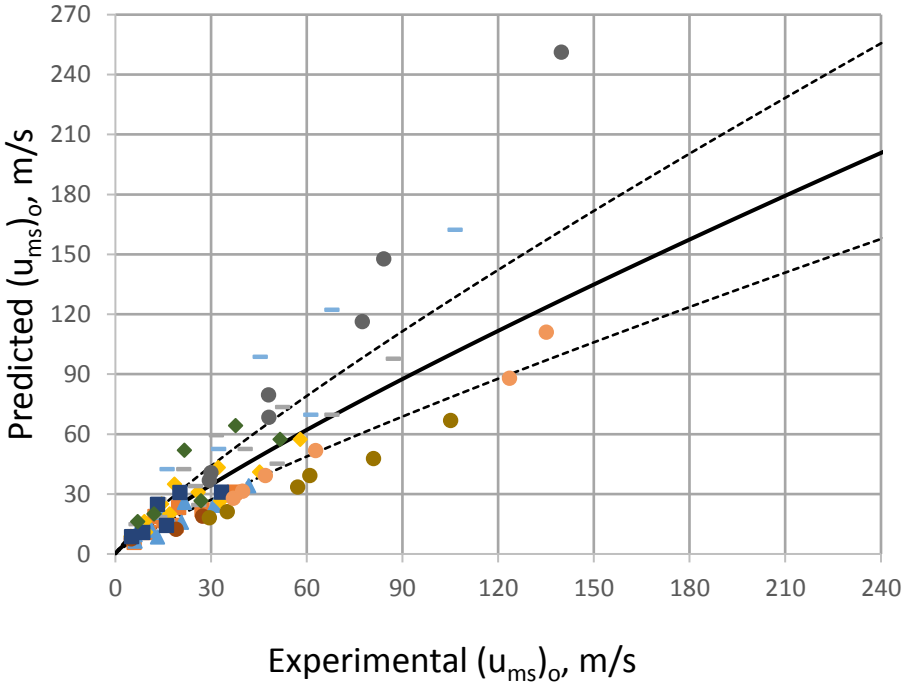

Figure 28: Choi Correlation

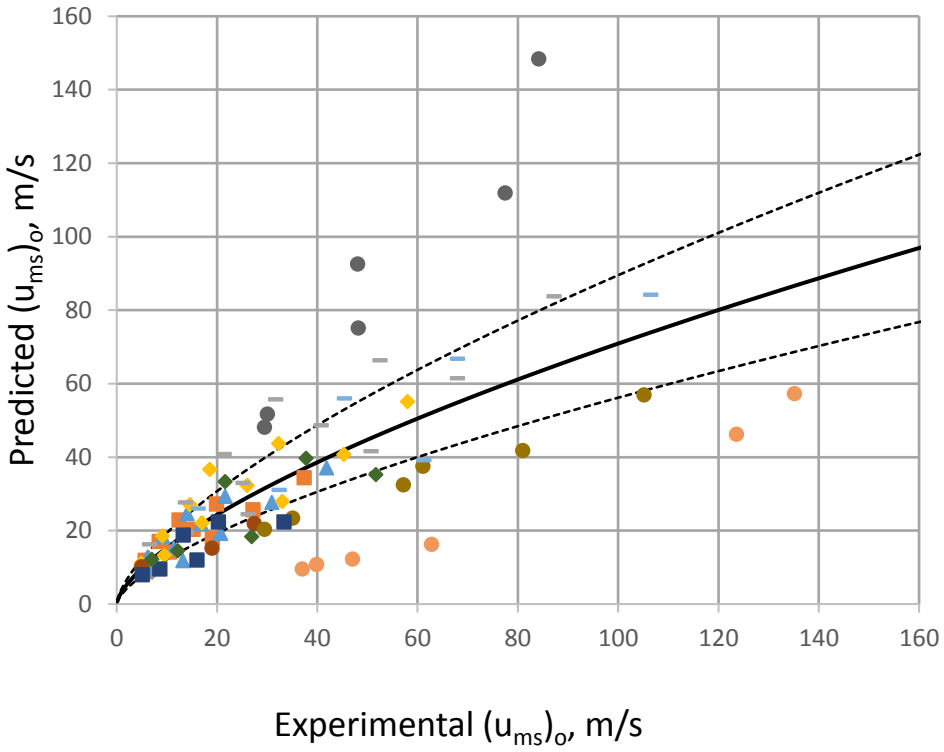

Figure 29: Bi Correlation

While the curve fits provide a visual understanding into the applicability of the fits and their precision, they lack clarity in the accuracy with respect to unity. To get an idea of the total error, a paired t-test was performed as described in Section 3.7. Larger the t-value indicate a less accurate the fit. The probability of the difference is also shown which is a function of the t-value. Smaller p-values (< 0.001) indicate that there is more certainty that there is a statistical difference between the correlations.

Table 7: Correlation Error

Source	$[(U_{ms})_{cor.} - (U_{ms})_{meas.}]_{avg.}$	Standard Deviation	t-value	p-value
Gorshtein (1964)	-19.312	23.646	-7.485	6.8×10^{-11}
Mukhlenov (1965)	13.513	27.230	4.548	1.43×10^{-17}
Tsvik et al. (1967)	-1.972	18.535	-0.975	1.55×10^{-18}
Olazar et al. (1992)	21.708	34.621	5.747	1.56×10^{-15}
Olazar et al. (1996)	-17.823	20.981	-7.786	2.94×10^{-14}
Bi et al. (1997)	0.849	22.194	0.350	1.76×10^{-16}
Choi (1992)	6.251	21.388	2.679	4.9×10^{-15}
Markowski (1983)	-3.531	19.711	-1.642	4.27×10^{-19}

As seen in Table 7, the largest p-value is $6.8*10^{-11}$ meaning that there are far too significant differences between the correlations and measured data to accurately predict future data points. Thus, a new correlation is required and will be discussed in the following section.

4.4 Parameter Correlations

With other correlation now deemed insufficient to represent the current data, a correlation must be found to summarize the results. Similar to the previous correlations, a power law fit will be used and will resemble the structure shown in Equation 8 in which each parameter will be discussed. C, a, b, c, d, and e represent the exponential power law values to be determined from the experimentally found data. The terms were chosen by observing other empirically derived work found in Table 1, then trial and error to take care of the discrepancies from correlation to correlation. Additional terms were explored based on the Buckingham Pi theorem and one such term was found to significantly reduce the error [42]. Each term in Equation 8 will be discussed in the subsequent sections detailing why the term was chosen, the power law value and the physical meaning behind the behavior.

$$(Re_{ms})_o = 0.053\ (Ar)^{0.8} \left(\frac{H_0}{D_0}\right)^{1.36} \tan\left(\frac{\theta}{2}\right)^{.54} \varepsilon^{1.78} \tag{8}$$

4.4.1 Stagnated Bed Height and Inlet Diameter (H_0/D_0)

The term used to represent the stagnated bed height is nondimensionalized with the inlet diameter as done by Markowski, Gorshtein, Mukhlenov, and Tsvik [5, 2, 3, 4]. Based on the results shown in Section 4.1.2, it is expected that the power law value will be greater than 1 indicating that as the height grows, the required momentum needed for spouting increases non-linearly. The power law value is 1.3551 giving the expected value as greater than one. This contradicts Markowski who had power laws raised to 0.48 [5]. The information does seem to have stronger agreement with Tsvik and Mukhlenov who had power law values of 1.24 and 1.25 respectively [4, 3].

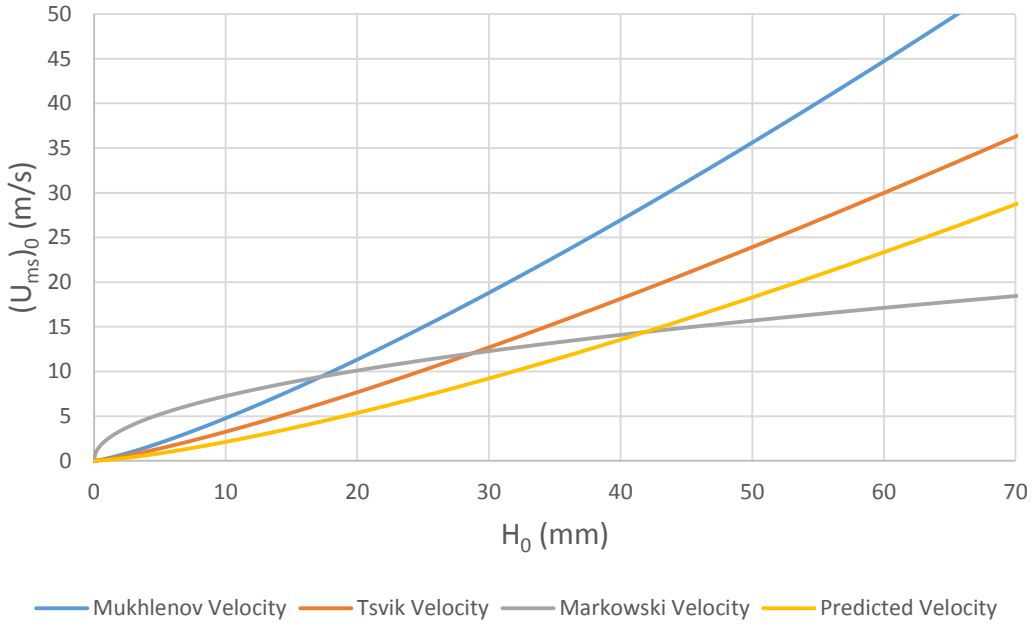

Figure 30: H_0 Power Law Comparison (D_0=6.35mm, θ=60°, d_p=686μm, Gas=Air, Aluminum Oxide Particles)

Intuitively, the power law should be greater than 1 as any lesser value would imply that less momentum is required over an increasing bed height as shown in Figure 30 in which the spouting velocity is measured as a function of bed height and other constant parameters. In this

figure, the Tsvik, Mukhlenov and current velocity seem to have agreement in the path, though the absolute values show deviation. The Tsvik velocity however, shows initial agreement, but will begin to diverge significantly at higher bed heights.

Having a power law less than 1 is counter-intuitive because the weight (or volume) of the particles should have a positive correlation with the spouting velocity. Further, the weight (or volume) of the spouting media is proportional to the height cubed due to the diverging nozzle; therefore, the spouting velocity would need to be proportional to less than 1/3 the power of the weight for this to be true, which is an intuitively low value.

The inlet diameter was also analyzed to have a negative correlation with the spouting velocity. This is expected because an increase in the inlet diameter, and therefore inlet area requires a velocity decrease to hold the equivalent momentum needed to maintain the spout. Though the momentum is not expected to hold at the exact same value as other parameters are changing, a general trend can still be expected.

The stagnated bed height was initially hypothesized to be combined with the inlet diameter for a nondimensionalized term. This was verified by separating the terms as other correlation have done using the cone diameter which led to Equation 9. It can be seen that both values share similar power law values leading to the change in total error being insignificant between the use of either term. The H_0/D_0 term was inevitable used based on its conciseness.

$$\left(\frac{H_0}{D_0}\right)^{1.36} \sim \left(\frac{H_0}{D_c}\right)^{1.39} * \left(\frac{D_c}{D_0}\right)^{1.33} \tag{9}$$

4.4.2 Solid-Gas Properties

The solid particle and fluid properties make up the majority of terms found in the correlation with the Archimedes number (Ar), non-diminsionalized particle diameter (d_p/D_0) and

the stagnated bed voidage (ε). The fluid properties are completely summarized by the Archimedes number in conjunction with the solid particle properties. However, it was found that addition properties beyond the Archimedes number were required to describe the interaction created by the solid particles. Each of these terms will be discussed in the sections below.

4.4.2.1 Archimedes Number

As discussed previously, the solid-gas properties are consolidated into one term – the Archimedes number. The Archimedes number, shown in Section 2.5 is proportional to the gas density and particle density while inversely proportional to the fluid viscosity squared .This aspect is the most consistent term included in the determination of spouting velocities across the literature with the power law ranging from 0.33-0.57. The exponential power law fit constant was found to be 0.8, higher than previous correlations found.

$$(u_{ms})_o \sim \rho^{-0.2} \tag{10}$$

$$(u_{ms})_o \sim \mu^{-0.6} \tag{11}$$

Equations 10 and 11 show the relationship between the spouting velocity and fluid properties based on the Archimedes and Reynolds number. For the fluid density, this result is expected as a reduction in density should result in an increase in the required velocity to achieve the same momentum since the momentum has a positive correlation with density and velocity. With the small ranges of viscosities used (1.81 – 2.23 *10^5 Pa s), it would be unlikely that it is playing a role in the Archimedes number compared to the larger parameter ranges of d_p, ρ, and ρ_p. However, the result is still expected – as the viscosity decreases, the shear stress will decrease

at the fluid-particle interface therefore, requiring a higher velocity to achieve the same momentum required for spouting.

4.4.2.1 Particle Diameter

From a classical perspective, choice in spouting media affects the spouted bed through the two physical parameters of density and particle size. These two parameters are generally taken into account by the Archimedes number (with the exclusion of Choi) [2, 3, 4, 5, 6, 7, 8, 9]. Upon inspection of the Archimedes number, the ratio of the exponents of d_p and ρ_p is 3 assuming that $\rho_p >> \rho$. This means that the particle size effects can outweigh the density in the correlation and has been studied by Olazar [7, 51]. To examine this for the current study, the additional term of d_p/D_0 was considered in which the power law value is 0.097. Without the addition of this term, an average error of 0.2% would be added across the 84 data points which shows a small necessity for the term and was not used due to over parameterization. This affirms the idea that the Archimedes number properly characterizes all solid particle interactions except for the stagnated bed voidage to be discussed below.

$$(u_{ms})_o \sim d_p^{1.4} \tag{12}$$

Equation 12 shows the relationship between the mean particle size and the spouting velocity. The particle size has a similar relationship to the height in that as the size and weight of each particle increases, the momentum required for spouting will increase at a rate larger than each independent variable.

4.4.2.2 Stagnated Bed Voidage (ε)

While the bed voidage is discussed in the literature, it is not commonly used in spouting velocity correlations. The stagnated bed voidage (ε) was added based on the author's intuition to

take into account the difference in packing between the aluminum oxide and porcelain particles and is therefore defined as:

$$\varepsilon = \frac{\rho_b}{\rho_p} \tag{13}$$

where ρ_b is the density of the particles in their packed state which accounts for the air in the gaps of the spouting media. ε should therefore, range between 0 and 1.

Though the bed voidage is a function of the particles (ρ_p), ρ_b is dependent on the sizes and shapes of the particles. Therefore, the way the particles pack is based on the distribution of the particle sizes and shapes which is what this term will take into account. Four values were recorded and are summarized in Table 8.

Table 8: Stagnated Bed Voidage Values

Particle	d_p (mm)	ε
Aluminum Oxide	0.483	0.5763
Aluminum Oxide	0.686	0.5503
Aluminum Oxide	1.092	0.5767
Porcelain	1	0.6622

Figure 31: Porcelain Spouting Media

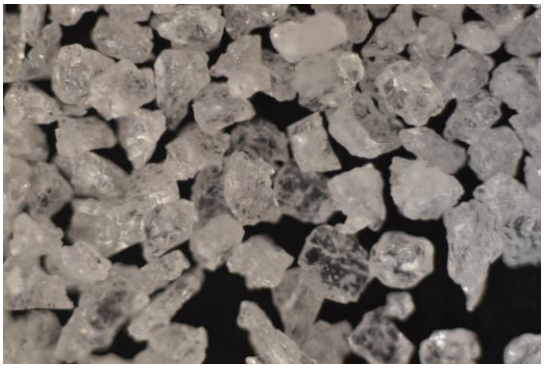

Figure 32: Aluminum Oxide Spouting Media (d_p=1.092mm)

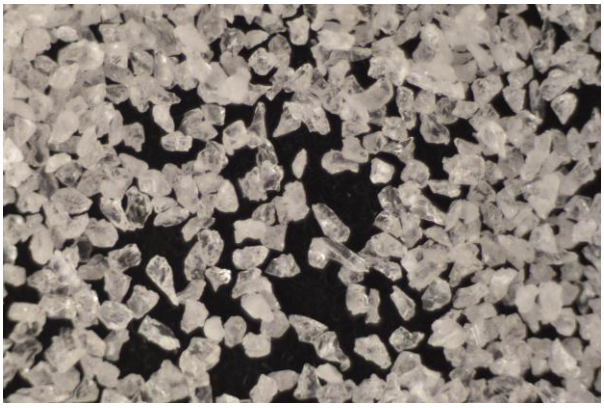

Figure 33: Aluminum Oxide Spouting Media (d_p=0.483mm)

It is evident that the porcelain has less gaps between the particles than the aluminum oxide. This is most likely due to a larger distribution of particle sizes. Figure 31 – 34 show a range of the particle sizes used. The porcelain particles have a well characterized spherical shape while the aluminum oxide does not. The porcelain seems to have a wider distribution of particle sizes however, allowing the smaller particles to fit into the crevasses between larger particles thus having a larger ε.

With the addition of this term, the exponential value found for the stagnated bed voidage was found to be 1.781. Since the stagnated bed density (ρ_p) will be influenced most heavily by the distribution of smaller particles, it seems that this effect is the driving force behind this term making the distribution of particle sizes a significant factor.

4.4.3 Cone Angle

The final term to be analyzed is the cone angle, which is most commonly represented as the tangent of half of the cone angle. This is often referred to as the coefficient of internal friction and represents the ratio of the bed height diameter by the stagnated bed height. The coefficient of internal friction represents the normal force provided by the CSB structure.

The correlation found is expected to be positive and be less than 1. As the cone angle increases, the amount of particles that can be fit into the system for the same operating conditions can increase, therefore increasing the required spouting velocity. As the cone angle approaches larger angles though, the spout will be less dependent are the particles to the edge of the system as the re-circulatory value will be weak thus making the power law value less than one. The exponential value found for the power law value was an expected value of 0.5433. The cone angle can also be written as shown in Equation 14 as a function of the spouting media where D_b is the diameter at the bed height.

$$(u_{ms})_o \sim \tan^{0.54}\left(\frac{\theta}{2}\right) = \left(\frac{1}{2}\frac{D_b - D_0}{H_0}\right)^{0.54} \tag{14}$$

4.4.4 Correlation Error

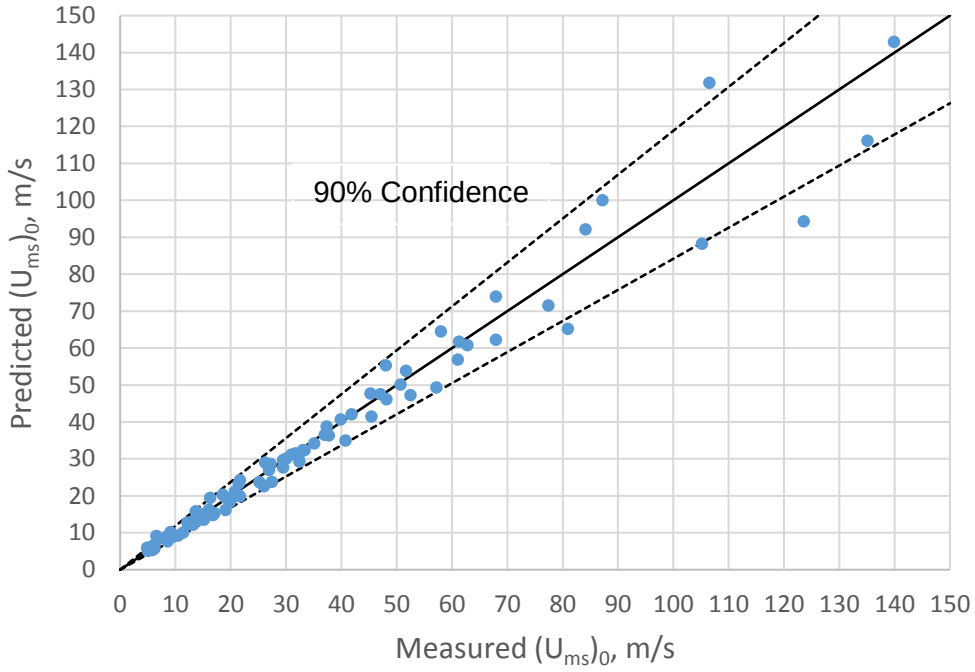

Figure 34: Correlation Error with 90% Confidence Interval

While the correlation presents the best found model for the data, error is still present though not as significant as found in other correlations. Figure 34 shows the predicted minimum spouting velocity determined from the correlation as a function of the measured values with a 90% confidence interval. The maximum error is 38.8% while the minimum is -23.8%. While the minimum error is slightly above the range of expected engineering error, the maximum error is much too high. However, the value represented as 38.8% error is one of the smallest recorded Reynolds numbers making any fluctuation be felt especially harsh. Figure 35 shows a breakdown of the error found in the 84 data points in which 73 points of the data (87%) falls within a standard engineering error of 15%. The total error is represented by the summation of all error is 685% giving an average error of 8.2%.

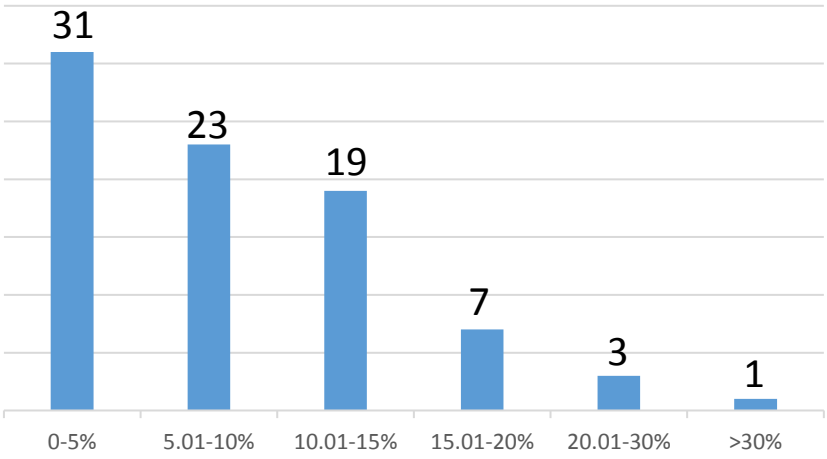

Figure 35: Correlation Error

It should be noted that while the maximum and minimum error can be dominated by small data points, the confidence interval is dominated by larger data points with the five largest points in Figure 34 making up 81.8% of the standard deviation, or interval observed.

4.4.4.1 Particle Density Uncertainty

The manufacturer reported density (McMaster-Carr) for the aluminum oxide and porcelain were both found to have errors after testing. The aluminum oxide density was reported as its solid state of 3950 kg/m^3. After examination, it was found that there were pores inside the particles causing the density to be less than the reported value. The internal porosity (ρ_p/ρ_{Al2O3}) was found to range between 0.85 – 0.89. While there is no porosity in the porcelain particles, it was found that the reported density was incorrect by 400 kg/m^3.

Because this was discovered late in the design process and the laboratory scale was malfunctioning, a low resolution (±.5g) scale was used to roughly determine these values thus presenting additional error in the correlation.

4.5 Correlation Comparison to Previous Study

Table 3: Parameter Comparison Between the Previous and Present Study [31]

Source	Particle size (mm)	Particle Density (kg/m^3)	D_0 (mm)	D_c (mm)	θ (deg)	H_o (mm)	Gas
Previous Study	0.483, 1.092	3920	3.302, 4.572, 6.35	69.9	60	10 - 50	Air
Present Study	0.483, 0.686, 1.0, 1.092	2002, 3920	3.30, 4.47, 6.0, 6.35	69.9	45, 60	10 - 70	Air, Argon, Helium

As shown in Table 3, the parameter selection was increased significantly between the previous and present study. The effects of parameter selection can be observed more clearly by looking at the previous correlation (Equation 15) found from the parameters shown in Table 3 [31].

$$(Re_{ms})_o = 717.26\,(Ar)^{0.08}\,(H_o/D_o)^{0.85}\left(d_p/D_o\right)^{1.23} \tag{15}$$

One major difference that can be found is the coefficient the Archimedes number is raised towards which is a factor of 10 times less than the value proposed for the current study. This is related to the particle size which is a factor of 10 times larger than that of the current study. The cause of this difference is due to the Archimedes number only being varied as a function of the particle diameter since the particle density or fluid was never changed. Therefore, particle effects were only placed in the d_p/D_0 term as it was varied near independently of the Archimedes number. The current study changed these values between a wider range in which a multitude of variables are changing within the Archimedes number. The current study indicated that the Archimedes number is a better term to use to indicate spouting media properties compared to d_p/D_0.

Another interesting trend is that the coefficient found for H_0/D_0 is less than 1. This is interesting because data collected in the current study at the same conditions indicated a coefficient greater than 1 while Sharma's data shows that the data has correlations less than 1 [31]. It is likely that data measurements were less confident as a significantly smaller amount of data points were taken and were done manually compared to the autonomous system used in the current study.

Two terms were not included being the term relating cone angle (θ) and the stagnated bed voidage which would be frivolous in the previous study as these terms were not varied.

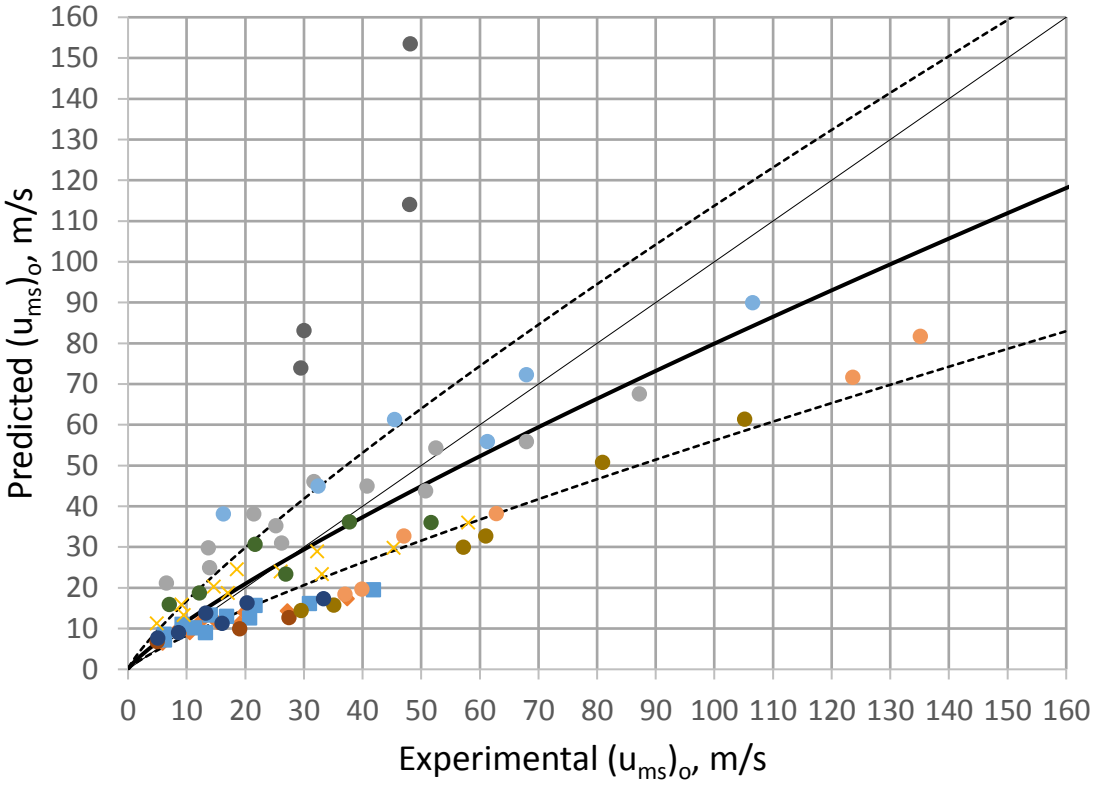

Figure 36: Sharma Correlation

The graphical representation as shown with other correlations can be seen in Figure 36. As seen, the 50% confidence interval is substantial as well as the p value which is 4.5×10^{-8}. While this p-value is better than any other correlations presented, it still shows no statistical

significance between the two correlations. This sharp contrast between results for CSBs of the same scale shows the importance of parameter selection and variance.

4.6 Spouting Instabilities

The three parameters presented in literature to achieve stable spouting were the ratios of D_i/d_p, D_i/D_0 and θ [14]. The first ratio of D_i/d_p was varied with a minimum of 3.024 and maximum of 13.147. Mathur had found that the ratio required for stable spouting was less than a value ranging from 2-60 – an uncertain claim at best [35]. However, with stable spouting found when operating in this region, the claim does hold and it seems the ratio may be on the lower end at a value closer to 2. Like most other aspects of the CSB, it is likely heavily influenced by the design and scale of the system.

According to Olazar, D_i/D_0 was tested in a marginally unstable range for all results as the ratio was kept as 1. Olazar stated that the value must lie between 0.5 and 0.83 for conclusive stable spouting while results are inconclusive outside of this range [7]. This deals with the agglomeration of particles in the discontinuity that separate D_i and D_0 values would create – but this was found to not affect the stability of the system under the current parameters. θ was not tested as previous work by Sharma found that instability occurred in the region predicted by the literature near 30° [31].

Instability was found however as a function of the gas used. When testing helium at D_0=3.30mm, d_p=0.483mm, θ=60° and at and H_0, the fountain periphery closed and opened rapidly creating an instability. Interestingly enough, the phenomenon faded as the particle diameter was increased to d_p=0.686mm and disappeared at d_p=1.092mm. The instability was tested for a range of bed height and found have no dependence. Even more interesting was that this phenomenon disappeared for all particle sizes used when the inlet diameter was increased to

and beyond D_0=4.468mm. A fluid to geometric interaction is therefore occurring causing the instability, most likely a function of (ρ, D_0, d_p). Due to the design, the instability occurred at the smallest D_0 and d_p available making further exploration impractical. It is the author's suggestion that this be further studied in future literature as no text could be found suggesting fluid to geometric stability issues.

4.7 Internal Spouting Trends

Internal spouting was suspected when experimentation first began due to the large pressure drops that were observed with a lack of spouting. This was later confirmed by using a transparent cone in which circulation occurred only at certain height less than H_0. Based on the presence of internal spouting, less significance is given to the pressure drop observed to attain stable spouting (breaking force friction) because the pressure drop required is not just a function of H_0, but a function of the remaining bed height to which the internal spout has not yet formed.

This is interesting as it can suggest that there may be circulation patterns available at speeds less than $(U_{ms})_0$. However, it was found that internal spouting trends are much less predictable than the external spout and will be discussed below.

4.7.1 D_0 and H_0

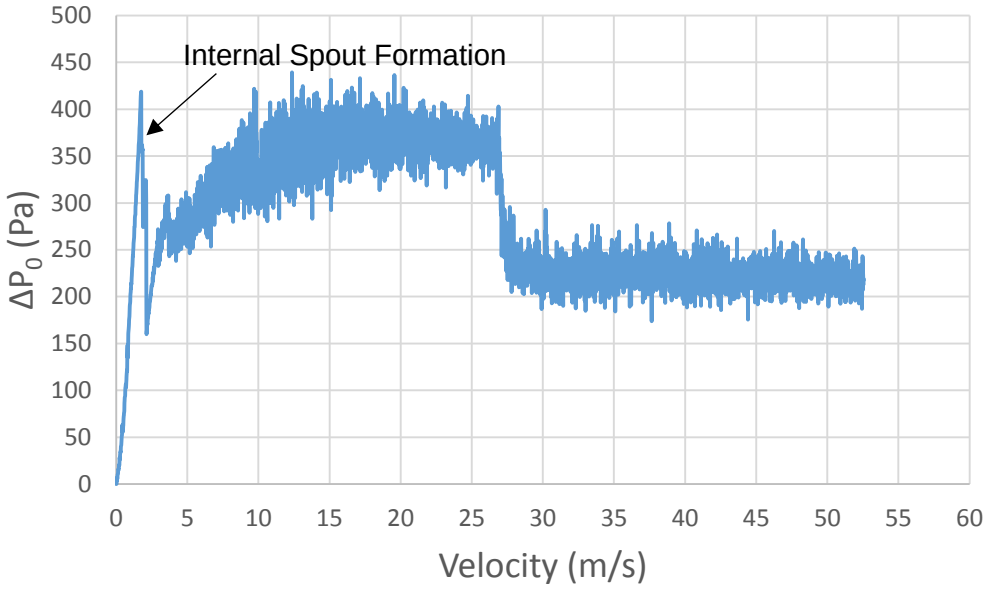

Figure 37: Unfiltered/Raw Pressure Curve for H_0=40mm, D_0=6.35mm, θ=60°, d_p=1092µm, Gas=Air, Aluminum Oxide Particles

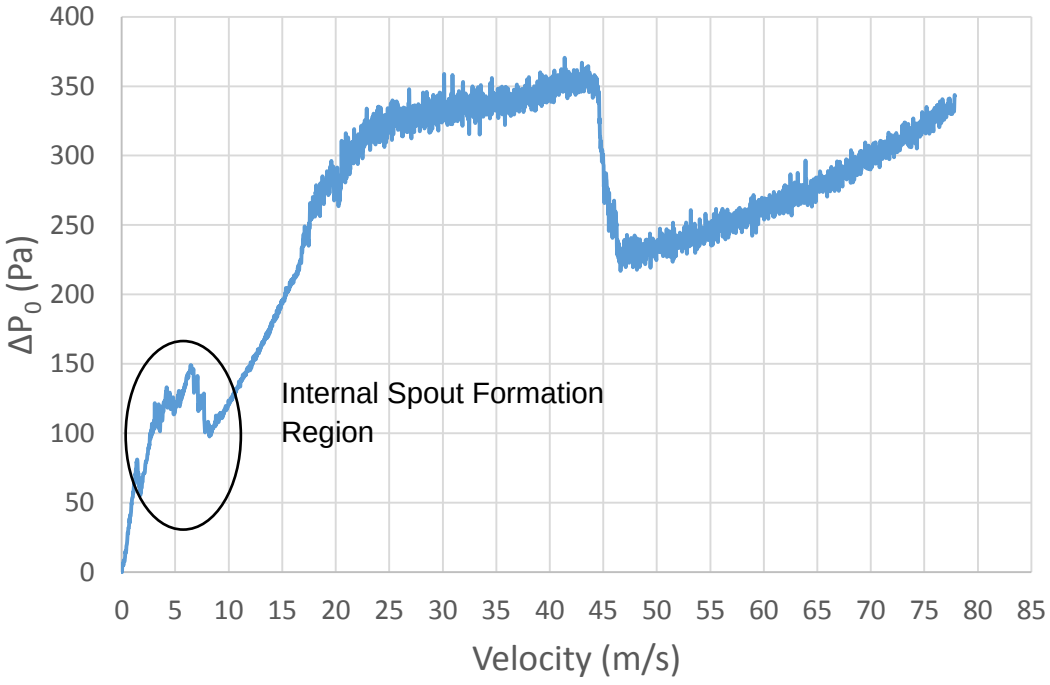

Figure 38: Unfiltered/Raw Pressure Curve for H_0=40mm, D_0=4.47mm, θ=60°, d_p=1092µm, Gas=Air, Aluminum Oxide Particles

Internal spouting can be seen in pressure curves as sudden increases in pressure (reading from right to left) from the spout collapsing to a certain height where the momentum is still sufficient to keep the rest of the spout formed. Therefore, larger jumps in pressure indicate a taller path cleared for internal spouting until the external spout is reached. The data is presented as the linearly corrected pressure recorded before sending the data through a low pass filter and removing the noise due to the filter often dampening the observed internal spouting. Figure 37 and 38 show examples of pressure curves with constant parameters excluding D_0. It seems that as D_0 decreases, more internal spouts can be seen at smaller degrees compared to the one major internal spout at 6.35mm leading to a negative correlation between internal spouting and D_0.

For H_0, it has been shown and noted in Section 4.1.1 that the internal spout is not a function of this parameter as it formed at the same position regardless of the bed height.

4.7.2 d_p

It seems that the particle diameter can also have an even more substantial effect than D_0. As seen in Figure 38 and 39, all parameters are kept constant excluding d_p. For the smaller particle diameter, there seems to be only one internal spout formed that is short lived compared to the multitude of internal spouts observed in the larger d_p value. This is most likely due to the larger weight per particle at larger sizes and thus, a positive correlation is established between d_p and internal spouting.

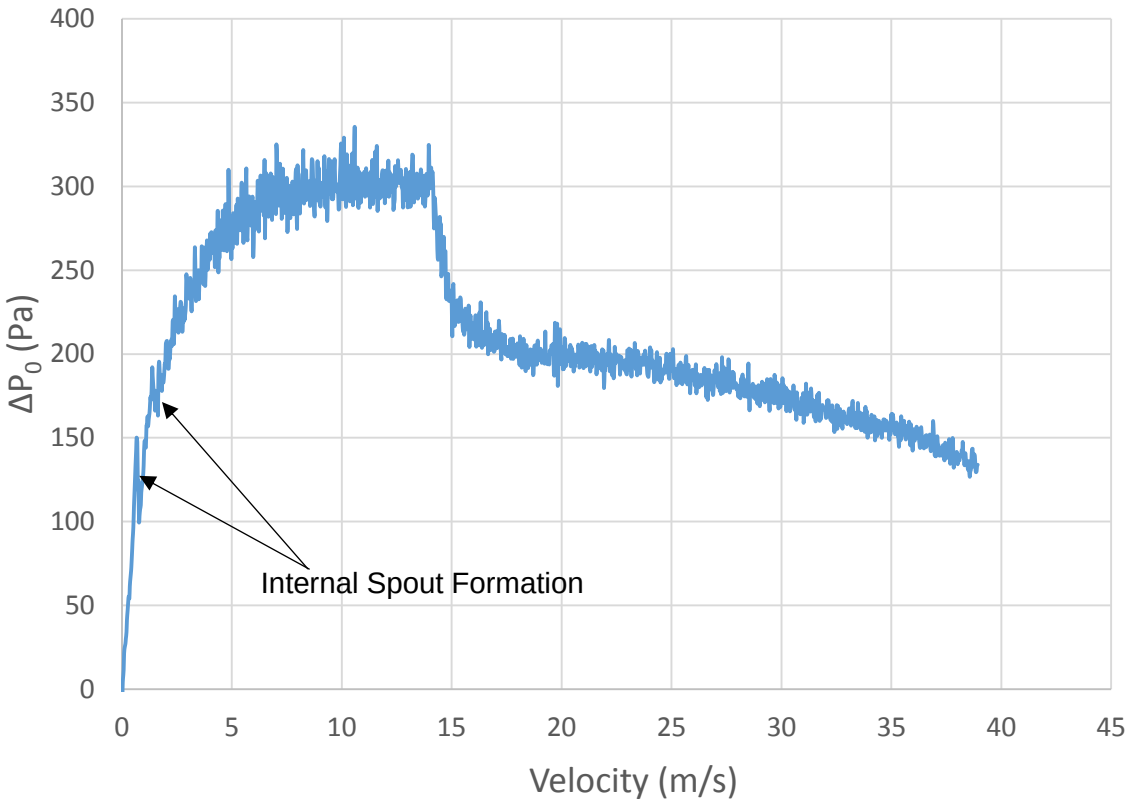

Figure 39: Unfiltered/Raw Pressure Curve for H_0=40mm, D_0=4.47mm, θ=60°, d_p=483μm, Gas=Air, Aluminum Oxide Particles

4.7.3 Effect of Particle Packing State

It could be said that there is an effect of the particle choice, represented by the density (ρ_p), but it is much more likely that differences observed between the porcelain and aluminum oxide particles are due to the different packing states and characteristic geometries. Figure 40 shows porcelain particles at the largest inlet diameter used which has two pressure increases indicating internal spouting. More interesting is Figure 41 in which the parameters are the same with the smallest inlet diameter being used. It seems that the pressure remained constant over a range of velocities (12m/s – 75m/s) giving a very different curve than yet observed. It is likely that the fluid was able to circumvent through the spouting media for a long range of velocities.

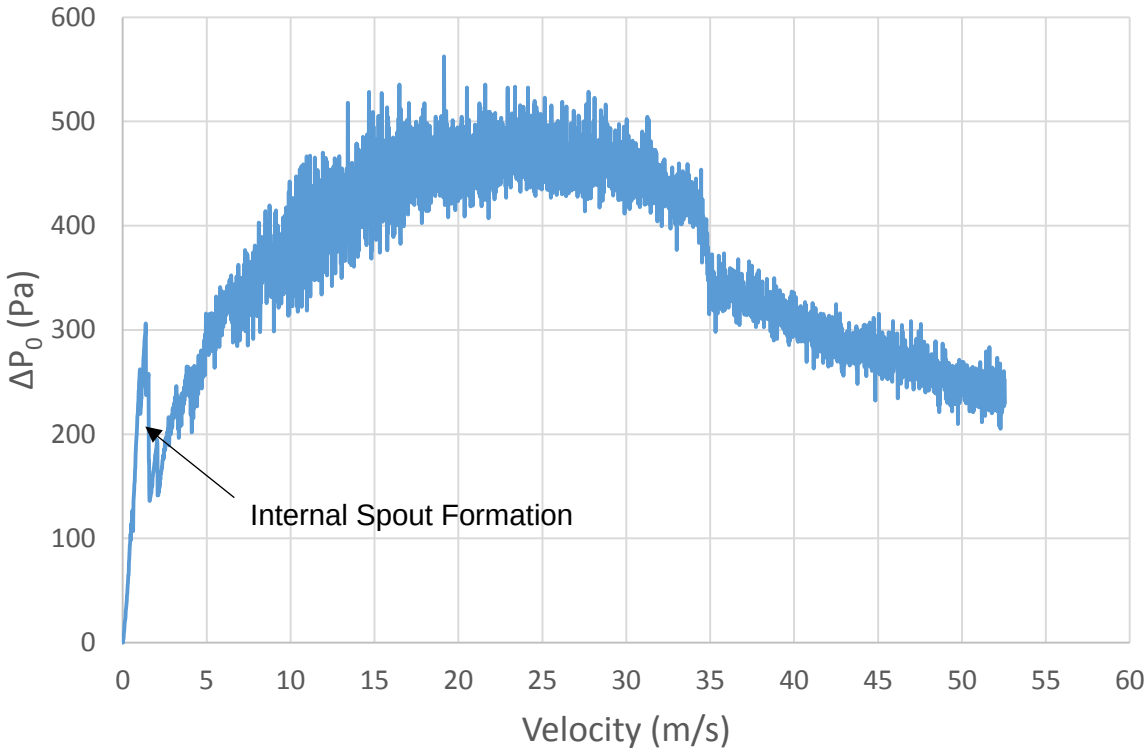

Figure 40: Unfiltered/Raw Pressure Curve for H_0=45mm, D_0=6.35mm, θ=60°, d_p=1000µm, Gas=Air, Porcelain Particles

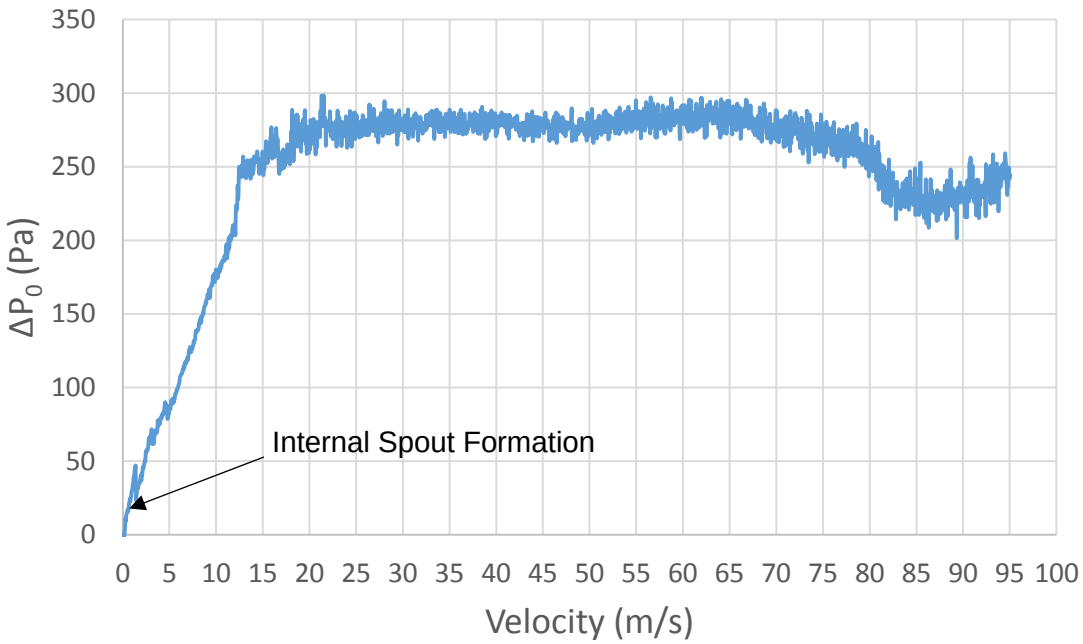

Figure 41: Unfiltered/Raw Pressure Curve for H_0=40mm, D_0=3.30mm, θ=60°, d_p=1000µm, Gas=Air, Porcelain Particles

It should be noted however, that internal spouting can still occur without a major visible effect in the pressure. If a spout forms slowly, its effect in the pressure may not be seen compared to larger spikes being indicative of a rapidly occurring spout. This implies that the formation of internal spouts is qualitative in nature.

CHAPTER 5
CONCLUSION

5.1 Conclusion

The purpose of the study was to develop a conical spouted bed with which to analyze its behavior at a small-laboratory scale. To test this, previous experiments were expanded on by use of an automated data acquisition system suitable for testing a multitude of parameters. The parameters varied include the stagnated bed height (H_0), inlet diameter (D_0), particle density (ρ_p), mean particle size (d_p), fluid density (ρ), fluid viscosity (μ), and cone angle (θ). Through the varying of these parameters over 84 test, a comprehensive correlation was created with an average error of 7.6%.

Other correlations were also explored detailing the uncertainty in the field between parameters chosen for the correlations and results. All correlations presented extensive error and had no statistical correlation when compared to the experimental results obtained for the current apparatus. This verified the need for a new correlation specific to the testing parameters.

A further goal of the study was to study the effects of gasses at low densities as to simulate elevated temperature conditions that would be experienced in the next phase of research involving a CSB reactor. Helium was chosen to accomplish this task by decreasing the density and viscosity. An average error of 6% is recorded across the low density measurements showing a sufficient correlation.

With the completion of this study and an elemental understanding of how parameters affect the flow in cold flow and simulated heated flow conditions, the next phase of the study can begin with recommendations for the study below.

5.2 Future Work and Recommendations

The results and proposed correlation provide a significantly better predictive method compared to other correlations as well as the difference in increasing parameter selection being shown. However, many factors lie ahead for the future work of using the CSB as a reactor. The first is in the CSB design and DAQ. The basic CSB geometry should be sufficient for use, though new pieces will need manufacturing as 3D printed plastic structures will not be able to withstand the high temperatures required in the reactor. A new method must also be used to secure the mesh that holds the particles from flowing upstream. It is recommended to use a hollowed metallic cylinder which is held in place by an internal retaining ring. The DAQ must also be updated to a new system. It is unlikely an Arduino will be able to handle the various needs of multiple thermocouples and flow meters required.

The stability of the system was also a factor that was not properly analyzed in the current study. Because instability was only found in low density gases (ρ=0.1664 kg/m3), the smallest inlet diameter (D_0=3.3mm) and the smallest particle size (d_p=0.483mm), studying further effects of the instability was out of the scope of the parameters used in the current study. However, it is recognized that the issue is a function of low density gases that will commonly be observed in the CSB reactor. Testing under these conditions should be monitored in the next study by a combination of visual determination in which oscillatory opening and closing of the spout will be apparent and by the pressure which will also oscillate heavily.

REFERENCES

[1] G. Elordi, M. Olazar, G. Lopez and J. Bilbao, "Catalytic Pyrolysis of HDPE in Continuous Mode Over Zeolite Catalysts in a Conical Spouted Bed Reactor," *Journal of Analytical and Applied Pyrolysis*, vol. 85, no. 1, pp. 345-351, 2009.

[2] A. E. Gorshtein and I. P. Mukhlenov, "Hydraulic Resistance of a Fluidized Bed in a Cyclone without a Grate. Critical Gas rate Corresponding to the Beginning of Jet Formation," *Zh. Prikl. Khim. (Leningrad),* vol. 37, pp. 1887-1893, 1964.

[3] I. P. Mukhlenov and A. E. Gorshtein, "Investigation of a Spouted Bed," *Khim. Prom.,* vol. 41, no. 6, pp. 443-446, 1965.

[4] M. Z. Tsvik, M. N. Nabiev, N. U. Rizaev, K. V. Merenkov and V. S. Vyzgo, "The Velocity for External Spouting in the Combined Process for Production of Granulated Fertilizer," *Uzb. Khim. Zh.,* vol. 11, no. 2, pp. 50-59, 1967.

[5] A. Markowski and W. Kaminski, "Hydronamic Characteristics of Jet-Spouted Beds," *Can. J. Chem. Eng.,* vol. 61, pp. 377-381, 1983.

[6] M. Choi and A. Meisen, "Hydrodynamics of Shallow, Conical Spouted Beds," *Can. J. Chem. Eng.,* vol. 70, pp. 916-924, 1992.

[7] M. Olazar, M. J. San Jose, A. T. Aguayo, J. M. Arandes and J. Bilbao, "Stable Operation Conditions for Gas-Solid Contact Regimes in Conical Spouted Beds," *Ind. Eng. Chem. Res.,* vol. 31, pp. 1784-1792, 1992.

[8] M. Olazar, M. J. San Jose, E. Cepeda, R. Ortiz de Latierro and J. Bilbao, "Hydrodynamics of Fine Solids on Conical Spouted Beds," in *Fluidization*, New York, Engineering Foundation, 1996, pp. 197-205.

[9] H. T. Bi, A. Macchi, J. Chaouki and R. Legros, "Minimum Spouting Velocity of Conical Spouted Beds," *Can. J. Chem. Eng.,* vol. 75, pp. 460-465, 1997.

[10] C. E. Robinson, "Improvement in Furnaces for Roasting Ore". United States Patent 212508, 1879.

[11] P. E. Gishler and K. B. Mathur, "Method of Contacting Solid Particles with Fluids". National Research Council of Canada Patent 2786280, 1957.

[12] P. E. Gishler, "The Spouted Bed Technique-Discovery and Early Studies at N.R.C.," *Can. J. Chem. Eng.,* vol. 61, pp. 267-268, 1983.

[13] K. B. Mathur and P. E. Gishler, "A Technique for Contacting Gases with Coarse Particles," *AIChE Journal,* vol. 1, pp. 157-164, 1955.

[14] N. Epstein and J. R. Grace, Spouted and Spout-Fluid Beds, New York: Cambridge University Press, 2011.

[15] M. Leva, Fluidization, New York: McGraw-Hill, 1959.

[16] N. I. Syromyatnikov, "Results of Tests on Furnaces of the Fluidized, Suspended and Spouting Types," *Za. Ekonom. Topl.,* vol. 2, pp. 17-21, 1951.

[17] S. C. Siu and J. W. Evans, "Efficient Electrowinning of Zinc from Alkaline Electrolytes". Unites States Patent 5958210, 1999.

[18] D. Geldart, "Types of Gas Fluidization," *Powder Technology,* vol. 7, no. 5, pp. 285-292, 1973.

[19] "Kurimoto," [Online]. Available: http://www.kurimoto.com. [Accessed 9 February 2017].

[20] V. Jiricny, J. Evans, W. Morgan, F. Dudek and M. Newman, "Berkeley," 1998. [Online]. Available: http://www.mse.berkeley.edu. [Accessed 14 March 2017].

[21] M. Olazar, M. San Jose, J. Bilbao, N. Epstein and G. R. John, "Conical Spouted Beds," in *Spouted and Spout-Fluid Beds*, New York, Cambridge University Press, 2011, pp. 82-104.

[22] O. Uemaki and T. Tsuji, "Gasification of a Sub-Bituminous Coal in a Two-Stage Jet Spouted Bed Reactor," in *Fluidization*, New York, Engineering Foundation, 1986, pp. 497-504.

[23] M. Olazar, M. J. San Jose, G. Aguirre and J. Bilbao, "Pyrolysis of Sawdust in a Conical SPouted Bed Reactor. Yields and Product Composition," *Ind. Eng. Chem. res.,* vol. 39, pp. 1925-1933, 2000.

[24] R. Aguado, M. Olazar, M. J. San Jose, B. Gaisan and J. Bilbao, "Wax Formation in the Pyrolysis of Polyolefins in a Conical Spouted Bed Reactor," *Energy and Fuels,* vol. 16, pp. 1429-1437, 2002.

[25] M. Arabiourrutia, G. Lopez, G. Elordi, M. Olazar, R. Aguado and J. Bilbao, "Product Distribution Obtained in the Pyrolysis of Tyres in a Conical SPouted Bed Reactor," *Chem. Eng. Sci.,* vol. 62, pp. 5271-5275, 2007.

[26] J. Bilbao, M. Olazar, A. Romero and J. M. Arandes, "Design and Operation of a Jet Spouted Bed Reactor with Continous Catalyst Feed in the Benzyl Alcohol Polymerization," *In. Eng. Chem. Res.,* vol. 26, pp. 1297-1304, 1987.

[27] M. Olazar, M. J. San Jose, F. J. Penas, A. T. Aguayo and J. Bilbao, "Stability and Hydrodynamics of Conical Spouted Beds with Binary Mixtures," *Ind. Eng. Chem. Res.,* vol. 32, pp. 2826-2834, 1993.

[28] M. S. Bacelos and J. T. Freire, "Flow Regimes in Wet Conical Spouted Beds Using Glass Bead Mixtures," *Particuology,* vol. 6, pp. 72-80, 2008.

[29] M. J. San Jose, M. Olazar, F. J. Penas and J. Bilbao, "Segragation in Conical Spouted Beds with Binary and Tertiary Mixtures of Equidensity Spherical Particles," *Ind. Eng. Chem. Res.,* vol. 33, pp. 1838-1844, 1994.

[30] M. L. Mastellone and U. Arena, "Fluidized-Bed Pyrolysis of Polyolefin Wastes: Predictive Defluidization Model," *AIChE J,* vol. 48, pp. 1439-1447, 2002.

[31] M. Sharma, M. Lousteau and I. Schoegl, "Hydrodynamic Study of Small-Sized Conical Spouted Bed," in *ASME Early Career Technical Journal*, Atlanta, 2011.

[32] M. Z. Tsvik, M. N. Nabiev, N. U. Rizaev, K. V. Merenkov and V. S. Vyzgo, "Minimal Rate of Internal Gushing During Composite Production of Granulated Fertilizers," *Uzb. Khim. Zh.*, vol. 10, pp. 3-6, 1996.

[33] W. F. Fung, P. G. Romankov and N. B. Rashkovskaya, "Research on the Hydrodynamics of the Spouting Bed," *Zh. Prikl. Khim.*, vol. 42, pp. 609-617, 1969.

[34] Z. G. Wang, H. T. Bi, C. J. Lim and P. C. Su, "Determination of Minimum Spouting Velocities in Conical Spouted Beds," *Can. J. Chem. Eng.* , vol. 82, pp. 12-19, 2004.

[35] K. B. Mathur and N. Epstein, Spouted Beds, New York: Academic Press, 1974.

[36] J. Kucharski and A. Kmiec, "Hydrodynamics, Heat and Mass Transfer During Coating of Tablets in a Spouted Bed," *Can. J. Chem. Eng.,* vol. 61, pp. 435-439, 1983.

[37] A. M. Nikolaev, L. G. Golubev and S. M. Kirov, "Basic Hydrodynamic Charecteristics of a Spouting Bed," *Khim. i Khim. Tekhnol,* vol. 7, pp. 855-857, 1964.

[38] M. Olazar, M. J. San Jose, A. T. Aguayo, J. M. Arandes and J. Bilbao, "Pressure Drop in Conical Spouted Beds," *Chem. Eng. J.*, vol. 51, pp. 53-60, 1993.

[39] N. I. Gelprin, V. G. Ainshtein and L. P. Timokhova, "Hydrodynamic Features of Fluidization of Granular Materials in Conical Sets," *Khim. Mashinostr.*, vol. 4, p. 12, 1961.

[40] Z. G. Wang, "Experimental Studies and CFD Simulations of Conical Spouted Bed Hydrodynamics," *Ph.D. Thesis, University of British Columbia,* 2006.

[41] F. Manurung, "Studies in the Spouted Bed Technique with Particular Reference to Low Temperature Coal Carbonization," *Ph.D. thesis, University of New South Wales, Kensignton, Australia,* 1964.

[42] P. Pritchard, Introduction ot Fluid Mechanics, New York: John Wiley & Sons, 2011.

[43] M. Olazar, M. J. San Jose, A. T. Aguayo, J. M. Arandes and J. Bilbao, "Design Factors of Conical Spouted Beds and Jet Spouted Beds," *Ind. Eng. Chem. Res.,* vol. 32, pp. 1245-1250, 1993.

[44] "TechSpecs," formlabs, [Online]. Available: https://formlabs.com. [Accessed 20 February 2017].

[45] "Arduino Uno," Arduino, [Online]. Available: http://www.arduino.org. [Accessed 20 February 2017].

[46] "Economical Gas Mass Flow Controllers," Omega, [Online]. Available: http://www.omega.com. [Accessed 20 February 2017].

[47] "adafruit," adafruit, [Online]. Available: https://www.adafruit.com. [Accessed 20 February 2017].

[48] "McMaster-Carr," McMaster-Carr, [Online]. Available: https://www.mcmaster.com. [Accessed 20 February 2017].

[49] "MathWorks," [Online]. Available: http://www.mathworks.com. [Accessed 2 July 2016].

[50] R. Shier, "Mathematics Learning Support Center," 2004. [Online]. [Accessed 20 March 2017].

[51] M. Olazar, M. J. San Jose, S. Alvarez and J. Bilbao, "Minimum Spouting Velocity for the Pyrolysis of Scrap Tyres with Sand in Conical Spouted Beds," *Powder Technology ,* vol. 165, pp. 128-132, 2006.

[52] P. P. Chandnani and N. Epstein, "Spoutabilitiy and Spout Destabilization of Fine," in *Fluidization*, New York, Engineering Foundation, 1986, pp. 233-240.

[53] C. J. Lim and J. R. Grace, "Spouted Bed Hydrodynamics," *Ca. J. Chem. Eng.,* vol. 65, pp. 366-372, 1987.

[54] M. Olazar, G. Lopez, H. Altzibar, R. Aguado and J. Bilbao, "Minimum SPouting Velocity Under Vacuum and High Temperature in Conical Spouted Beds," *Can. J. Chem. Eng.,* vol. 87, pp. 541-546, 2009.

[55] X. Bi, N. Epstein and J. R. Grace, "Initiation of Spouting," in *Spouted and Spout-Fluid Beds*, New York, Cambridge University Press, 2011, pp. 18-28.

[56] R. Figliola and D. Beasley, Mechanical Measurements, Hoboken: John Wiley & Sons, 2011.

APPENDIX
DATA ACQUISITION AND PROGRAMMING

An Arduino Uno was used as the central unit to control and read the experimental measurements. The devices used include a mass flow controller, pressure transducer, SD card reader and digital to analog converter. Each of these devices will be discussed below and how digital communication with Arduino proceeded. Figure 42 gives a visual representation with how digital communication took place.

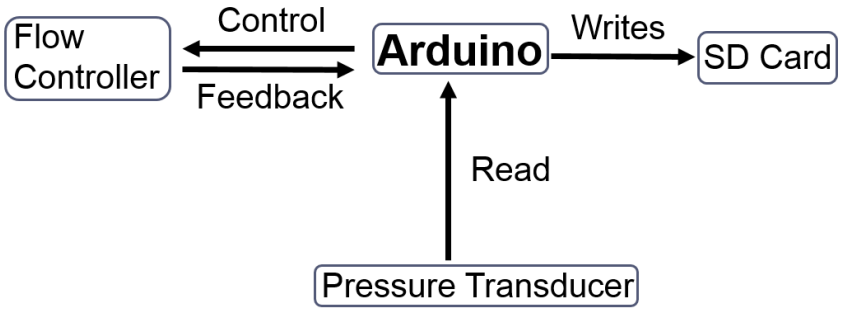

Figure 42: Block Diagram of DAQ System Communication

A.1 Mass Flow Controller

This device was one of the simplest devices to operate as it used basic Arduino functions. The flow controller was governed by the PWM (pulse width modulation) feature which pulses a digital signal at a high frequency to give a voltage output. PWM operators in integers between 0 (0 Volts) and 255 (5 Volts). The code was designed so that once the system was turned on, it would start at a flow rate of 0 and ramp up to a max flow rate (integer of 255) or a designated value. For example, most experiments did not need to achieve the maximum flow rate, so an integer less than 255 could be chosen as the max. Once the designated max flow was achieved, it would then ramp down back to 0. Time intervals existed between each integer so that a quasi-

equilibrium state could be reached. The time intervals could also be chosen independently in the ramping up and down process so that the process could be expedited as ascending (ramping up) data was not as useful in the current study.

Additionally, the mass flow controller had a read back feature. The values were read from the controller by using an analog pin in which 5 volts indicated a maximum flow rate of 100L/min and 0 volts indicated zero flow. The Arduino reads analog inputs as integers between 0 (0 volts) and 1023 (5 volts). For every data set, the commanded velocity and read back velocity were plotted and checked for agreement. In some cases, agreement did not occur usually due to an error which caused a discontinuity. These errors were usually short lived, meaning only 1 of the 5 test would be corrupted and could then be repeated.

Additionally, the mass flow controller, which was designed for Air as a working fluid, could be used for other gases, including the Helium and Argon used. A correction factor (K) was placed into the code and multiplied by the mass flow rate based on the gas. The K factor is given in the technical data by the manufacturer.

A.2 Pressure Transducer

The pressure transducer used was a barometric pressure sensor (SparkFun). Other gauge pressure transducers were initially experimented with, but were not used with the current experiment as the voltage output was too small and required an amplification factor of 600 – far too large to use without skewing data. Other pressure transducers were explored, but found to not provide a significant increase in resolution for the cost based on the design needs of the experiments. The pressure transducer was hermitically sealed in a PVC structure and connected to the Arduino. The transducer used a 3.3 volt power source and two analog pins over the I^2C interface. Open source code was modified to read the pressure directly instead of the altitude,

which the transducer was designed for. At this point, the data could be read and any further modifications, such as the conversion to the stagnated pressure, could be done after the initial data acquisition.

A.3 SD Card Reader

The SD card reader recorded 4 values during the testing process and stored them into a (.csv) file which could be read by Microsoft Excel. The first value was the read-back mass flow rate as a function of integers between 0 and 1023 which was rarely used. The next value was the absolute pressure. This pressure would later be converted to a gauge and corrected pressure as discussed in above. The final two values were the measured and set velocities. These were initially recorded a flow rates in the Arduino program and converted to velocities prior to being deposited onto the SD card. Therefore, the inlet diameter had to be specified in the code before beginning all test.

A.4 Digital to Analog Converter

The digital to analog converter allows increased resolution across the mass flow controller. Based on the Arduino pulse width modulation (PWM) that was used to govern the mass flow controller, it could be increased in integers ranging between 0 and 255, giving the controller a resolution of 0.4% of the total flow rate. Preliminary testing found that this was insufficient as too few data points were taken across the pressure drop observed at the spout formation. Therefore, a digital to analog converter (DAC) was used in which the resolution was increased to integers ranging between 0 and 4096 by using a 12 bit system, increasing the resolution from to 0.02% increments of the total flow rate.

A.5 Flow Rate of Change

An additional feature of the code not yet discussed is the time increments used to change the flow rate. The time desired is a point at which the system reached a quasi-equilibrium state while being the smallest possible amount for an expedited testing process. This time was found to be 300 milliseconds for each integer between 0 and 4096. This leads to the rate of change of the flow rate as 0.08 l/min per second.

Additional time delays were added at the beginning and end of the ascending and descending processes. A first delay was added for 20 seconds when the test began so that zero flow was established. The pressure was then taken at the end of this time which would be used to calculate the gauge pressure. At the end of the ascending process, the system was held at a constant flow for 10 seconds before beginning the descending process. Once the process reached zero flow, the 20 second time delay would be started again and the cycle would continue until halted.

A.6 Arduino Code

The code used to operate the Arduino is specified below. Note that comments (in gray) are placed throughout the code specifying the purpose of each part. Three aspects of the code were varied between each test which include the diameter and k value located in the beginning of the code as well as the initial voltage (max flow rate of system) at the end of the code.

```
//#include statements reference libraries
#include "SPI.h"
#include "SD.h"
#include "Wire.h"
#include "Adafruit_MCP4725.h"
#include "Adafruit_BMP085.h"

// list all variables

int MassFlowControllerAnalog = A1;   //Sets the analog output that reads the mass flow controller flow rate
int MassFlowRate = 0;                //Sets the initial mass flow rate
int fadeAmount = 1;                  //Defines the value that the flow will ramp up at. Must be a positive integer.
int delayAmount = 300;
int delayAmountDown = 300;
int RampUpMultiplier = 1.0;
float diamter = 6.35;                //Units in millimeters
float k = 1.454;                     //K factor is used so different gasses can be used through the flow controller.
                                     //K=1 when air or nitrogen is used. Reference K values in operating manual
uint32_t InitialVoltage;             //Defines the DAC output as InitialVoltage
const int chipSelect = 4;            //Sets pins for the SD Card

Adafruit_MCP4725 dac;                //Establishes use of the DAC
Adafruit_BMP085 mySensor;            //Establishes use of the pressure transducer
float pressure;                      //Establishes that pressure can be a changing value
float velocity_setpoint;             //Desired velocity
float velocity_measured;             //Actual velocity
File mySensorData;                   //Unsure on exact use. Used for the SD Card.

void setup() {

  // SD Card portion of code that establishes SD card pins and begins the writing
  mySensor.begin();
  pinMode(10, OUTPUT);
  SD.begin(4);
```

```
  //Begins the serial monitor so values may be viewed in real time
  Serial.begin(9600);

  // make sure DAC is working and outputs zero volt
  dac.begin(0x62);                          //Establishes the DAC address
  InitialVoltage = 0;
  dac.setVoltage(InitialVoltage,false);
  velocity_setpoint = 0.;

  delay(20000);
}


void loop() {

  // Prints the values to the serial moniter
  Serial.print("voltage = ");
  Serial.println(InitialVoltage);

  // Read Pressure
  pressure = mySensor.readPressure();

  // Reads the mass flow controller value
  MassFlowRate = analogRead(MassFlowControllerAnalog);

  // Prints the values to the serial moniter
  //Serial.print("massflowrate = ");
  //Serial.println(MassFlowRate);

  Serial.print("Pressure = ");
  Serial.println(pressure);

  //Mass Flow Rate Portion of Code
  InitialVoltage = InitialVoltage + fadeAmount;           //Establishes the ramping up of the voltage

  // If statement makes it such that the ramping up turns to ramping down at the specified value
  if (InitialVoltage <= 0 || InitialVoltage >= 4090) {
    fadeAmount = -fadeAmount ;
    delay (10000);
    mySensorData = SD.open("CSB.csv", FILE_WRITE);
    if (mySensorData) {
      mySensorData.print(""); //write empty line
      mySensorData.print(""); //write empty line
      mySensorData.print("changing direction");
      mySensorData.print(""); //write empty line
      mySensorData.println(""); //write empty line
      mySensorData.close();                                 //close the file
    }
  }

  // tell the DAC the desired voltage
  dac.setVoltage(InitialVoltage, false);

  // calculate velocity based on desired voltage (i.e. InitialVoltage)
  velocity_measured = k * 2.0744 * float(MassFlowRate) / sq(diamter); // replace by actual formula

  // writes data to the SD Card
  mySensorData = SD.open("CSB.csv", FILE_WRITE);
  if (mySensorData) {
    mySensorData.print(MassFlowRate);                     //write Mass flow rate to card (direct
    mySensorData.print(",");                              //write a commma
    mySensorData.print(pressure);                        //write pressure and end the line (println)
    mySensorData.print(",");
    mySensorData.print(velocity_measured);
    mySensorData.print(",");
    mySensorData.println(velocity_setpoint);              // need to lag value while we're waiting for 'equilibrated' data
```

```
  }

  // update *after* you wrote old value to SD card (lag behind to make data consistent)
  velocity_setpoint = k * .518094 * float(InitialVoltage) / sq(diamter); // replace by actual formula

  //Pause between readings.
  delay(delayAmount);


  if (fadeAmount > 0) {
    delayAmount = delayAmount / RampUpMultiplier ;
  }
  else {
    delayAmount = delayAmountDown;
  }
}
```

Vita

James Gegenheimer, son of David Gegenheimer and Kristen Gegenheimer, was born in 1993 in New Orleans, Louisiana. He attended Brother Martin High School in New Orleans where he earned his Diploma and LSU where he earned his Bachelor's degree in Mechanical Engineering in May 2016. Under Dr. Ingmar Schoegl, James began the accelerated master's program in June 2014.

James was commissioned in May 2016 as a Second Lieutenant in the United States Air Force with a Distinguished Graduate status. He will be stationed at Hill AFB in Salt Lake City, Utah for his first assignment and is pursuing a career in Research and Development.